AFIT/GEP/ENP/91D-2

(1)

AN ANALYSIS OF ONE-DIMENSIONAL MODELS OF THE INSULATING AND CONDUCTING PRIZ

THESIS

Joseph W. Cook, III, Captain, USAF

AFIT/GEP/~~ENG~~ENP/91D-2

AFIT/GEP/ENG/91D-2

AN ANALYSIS OF ONE-DIMENSIONAL MODELS OF THE INSULATING AND CONDUCTING PRIZ

THESIS

Presented to the Faculty of the School of Engineering

of the Air Force Institute of Technology

Air University

In Partial Fulfillment of the

Requirements for the Degree of

Master of Science in Engineering Physics

Joseph W. Cook, III, B.S.

Captain, USAF

December 1991

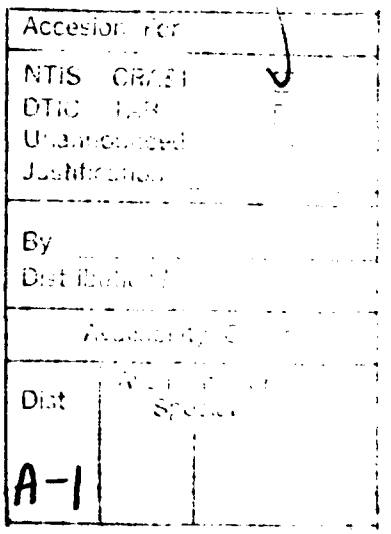

Approved for public release; distribution unlimited

Preface

The purpose of this study was to evaluate one-dimensional computer models for the insulating and conducting PRIZ. The PRIZ optical storage device offers great promise in the fields of optical computing and target detection. Both the Air Force Institute of Technology (AFIT) and the Foreign Technology Division (FTD) have sponsored research on the PRIZ since the early 1980's. The Soviet Union, however, has enjoyed, or at least reported, greater success in experimentally and analytically studying the PRIZ than we. This thesis is one of several produced at AFIT in attempts to duplicate reported Soviet results.

Dr. Theodore Luke, my thesis advisor, has coordinated all previous AFIT investigations into the PRIZ. A great portion of my time was spent simply catching up with the wealth of information he has accumulated over the years. I do not claim to understand all the work that has gone before me, but I credit Dr. Luke with helping me to narrow the scope of this thesis to the point where I can profess some expertise in my particular subject area. I especially appreciate his patience in guiding a computer-illiterate helicopter jockey through a computational thesis. I also appreciate the guidance provided by Dr. William Bailey, one of my thesis committee members, who often helped me to see forest and trees at the same time. Finally, I thank my newlywed wife Jennifer for selectively supporting and ignoring me at the appropriate times.

Joseph W. Cook, III

Table of Contents

List of Figures

List of Tables

List of Symbols

Roman Symbol	Definition
D'	Electric displacement (C/cm^2)
d_0'	Device thickness (cm)
$\mathscr{E}'$	Total exposure energy (J/cm^2)
e	Elementary charge (C)
E'	Electric field intensity (V/cm)
$E_0(t)'$	Electric field at cathode at time t (V/cm)
$E_j(t)'$	Electric field at end of bin j at time t (V/cm)
g'	Generation coefficient ($cm^{-2} \cdot sec^{-1}$)
G'	Generation rate (sec^{-1})
H'	Magnetic field intensity (Amp/cm)
h	Planck's constant (J•sec)
I'	Write light intensity ($Watts/cm^2$)
J_c'	Conduction current density ($Amps/cm^2$)
J_d'	Displacement current density ($Amps/cm^2$)
J_{diff}'	Diffusion current density ($Amps/cm^2$)
J_t'	Total current density ($Amps/cm^2$)
n_+'	Density of ionized donors (cm^{-3})
n_-'	Density of ionized, or filled, traps (cm^{-3})
n_0'	Concentration normalization factor (cm^{-3})
nbin	Number of discrete and equal slices of d_0'
N_d'	Density of donors (cm^{-3})
n_e'	Density of free electrons (cm^{-3})
$n_{e0}(t)'$	Electron density at the cathode at time t
n_s'	Injection coefficient of cathode (cm^{-3})
N_t'	Density of traps (cm^{-3})
t'	Time (sec)
t_0'	Initial transient time, or time constant (sec)
t_{exp}'	Exposure time (sec)
$\Re$	PRIZ response
V_0'	Applied external voltage (Volts)
z'	Longitudinal distance or crystal depth (cm)

Greek Symbol	Definition
η	Quantum efficiency
α'	Absorption coefficient (cm^{-1})
ϵ	Permittivity (F/m)
ϵ_0	Permittivity of free space (F/m)
ϵ_r	Relative permittivity
ζ_d'	Donor recombination coefficient (sec/cm^3)
ζ_t'	Trap recombination coefficient (sec/cm^3)
μ	Mobility of electrons ($cm^2/V \cdot sec$)

ρ'	Charge density (C/cm^3)
τ_d'	Average electron drift time (sec)
τ_t'	Average ionized trap lifetime (sec)
ν'	Write light frequency (Hz)

The prime notation (′) indicates dimensional variables that will be normalized, or used in the normalization process. The normalization process is contained in Table 1, page 27. Dimensional units such as e, h, ϵ, and μ that represent well known physical constants or specific material parameters do not carry the prime notation. Vector quantities are denoted by bars as in $\overline{E}$.

Abstract

This study attempted to analytically reproduce experimental and analytical data, on the single-insulated and conducting PRIZ, presented in 1987 and 1988 by the Soviet scientists Bliznetsov et al. Our one-dimensional analytical models, derived from earlier Soviet reports, have consistently reproduced previously reported data on the PRIZ. In this study, the same codes were successfully used to analyze the effects of injection at high and low intensity exposures (30 $\mu W/cm^2$ to 500 mW/cm^2). Although the codes qualitatively duplicated the nature of the space charge distribution in the single-insulated and conducting PRIZ, our quantitative results were significantly different from the Soviets'. Furthermore, the one-dimensional codes proved insufficient to effectively duplicate experimental data on reciprocity, self erasure, and regeneration. Specifically, we were unable to analytically reproduce Soviet experimental data establishing a reciprocity region for low exposures (< 20 $\mu J/cm^2$) in the conducting PRIZ. Since the basis for PRIZ operation, the linear electrooptic effect, is inherently a multi-dimensional phenomenon, we were not surprised to find some limitations to our one-dimensional models. Our results should serve as a basis for the development of more advanced two-dimensional analytical models of the PRIZ.

AN ANALYSIS OF ONE-DIMENSIONAL MODELS OF THE INSULATING AND CONDUCTING PRIZ

I. Introduction

The PRIZ is an optical storage device that offers great promise in optical computing and image processing. The term PRIZ is a Soviet acronym for Preobrasovatel Izobrazheniya which translates to "image transformer" (32:343). This study will investigate computer models of various configurations of the PRIZ. The output from these models will be compared to previously reported experimental and analytical work, and the results of these comparisons will be used to further our understanding of the basic physical processes governing the operation of the PRIZ.

The PRIZ consists of a single crystal of photorefractive material mounted between two transparent electrodes which are biased at several kilovolts. A writing light beam impinges on the crystal through one of the transparent electrodes. In general, the write light is perpendicular to the crystal face and impinges from the direction of the negative electrode, although other configurations have been used. The write light ionizes donor sites within the crystal releasing electrons that drift in the external field, producing a photocurrent. Some of the conduction electrons are captured by traps within the crystal prior to reaching the anode. The ionization of fixed donors, drift of

photoelectrons, and capture of electrons by fixed traps produces a space charge that varies with time and distance along the longitudinal axis of the crystal. The space charge will also vary along the transverse dimensions of the crystal, depending upon the characteristics of the writing-light intensity cross section and length of exposure. The transverse electric fields that are produced by this nonuniform charge distribution serve to modulate a reading-light beam that follows the writing-light through the crystal. The read light is of much lower photon energy than the write light, and therefore, is assumed to have an insignificant effect on the space charge produced by the write light. The formation of a space charge, which produces electrooptic modulation of the read light, is the physical basis of the PRIZ.

The PRIZ is fabricated in three configurations. These are the double-insulating (DI) PRIZ, the single-insulating (SI) PRIZ, and the conducting PRIZ. In the DI PRIZ, both electrodes are shielded from the crystal by transparent insulators that prohibit any injection or depletion of charge within the crystal. The SI PRIZ has an insulator at the cathode preventing injection, but no insulator at the anode. The conducting PRIZ has no insulators and therefore allows charge injection and extraction into and from the crystal through the external circuit. These differences profoundly influence the properties of the PRIZ in some operating modes while having little effect in other modes. To further complicate matters, PRIZ crystals cut from different bulk samples can exhibit widely varying properties (5:751).

As mentioned above, the PRIZ has several operating modes. Though not all-inclusive, three of these modes are image framing, dynamic image selection (DIS), and latent imaging. In the image framing mode, which is of great interest in optical computing, a write light is turned on then off. After a suitable time for image development, a read light is turned on, and the resulting modulated image is observed. The read light is then turned off, and an erase beam is injected into the crystal, while the electrodes are shorted, to redistribute the space charge homogeneously throughout the crystal. The complete read-write-erase cycle is called a frame. As reported by Casasent et al. in "Applications of the PRIZ Light Modulator", write times can be as short as 7 nsec using a pulsed laser source. Casasent continues with, "In this case, photocarriers were generated in a negligible time, but the output light pattern was not visible until 1 μsec later, and it peaked after 10 μsec." Casasent also reports that for "more conventional" exposure times of 1 msec, the output image is "immediately visible" (20:3847). The PRIZ can not be written again until electrons excited by the erase beam are redistributed and relaxed. Erasure times are on the order of 1 msec, and one millisecond of relaxation time is generally adequate before commencing a new frame (20:3847).

The framing mode reveals great initial insights into the inner workings of the PRIZ and the time intervals involved. In experiments, Casasent reports repetition rates of 20 frames/sec and image storage times of tens of seconds to one minute (20:3847). In a survey paper, the Russian scientist Petrov reports repetition rates of 30 frames/sec

for Bismuth Silicate ($Bi_{12}SiO_{20}$), one of the more common materials for PRIZ crystals (32:345). The reader who is interested in the specific means by which optical computing is engineered from a PRIZ is referred to "The Programming System PRIZ" by Mints and Tyugu (27:359).

A second mode of operation is dynamic image selection (DIS). This mode offers great potential to the Air Force in the form of a moving target detector. In this mode, a conducting PRIZ is written and read simultaneously and continuously, while a constant voltage bias is applied to the electrodes. When the write light is turned on, the modulation of the read light peaks and then decays to zero. In other words, the image written into the crystal progressively develops and then deteriorates until the image disappears. Because of this effect, images of stationary objects, which present a constant write light intensity to the crystal, are suppressed. Images that introduce changing intensities to the crystal, however, are enhanced. This enhancement can increase the ratio of moving image intensity to stationary image intensity by a factor of 20 (32:346). The PRIZ in DIS mode will also regenerate a suppressed stationary image when the write light that produced the image is turned off. The underlying physical basis for the phenomena observed in dynamic image selection is a topic of intense investigation and will be studied here to the extent one-dimensional techniques allow. The DIS mode of operation brought the conducting PRIZ to the forefront of PRIZ investigations.

The final mode of operation is the latent imaging mode. In this mode a latent image is recorded in the crystal by illuminating the

crystal while the voltage bias is set to zero. Although the resulting image can not be immediately read, subsequent application of a voltage bias and illumination with a suitable read light allows the latent image to emerge. Since this mode offers little additional insights to the PRIZ at this early stage, we will not elaborate. The interested reader is referred to Petrov (32:348).

The great versatility and potential of the PRIZ should be obvious from the preceding discussion. Still another advantage of the PRIZ is its inherent low noise level (32:343). With these advantages in mind, however, we must remember that the PRIZ is a very complicated device that begs intense and tedious investigations. One very significant problem is highlighted well by Shlyagin, et al. in "Mechanisms of Nonlinearity in a PRIZ Space-Time Light Modulator". In the first paragraph of this article, he states, "Space-time light modulators are used in optical data processing systems to input the signals to be analyzed. In general, it is desirable for the control and output signals of the modulator to be linearly related." (37:68) In the final paragraph, he confesses, "We have thus shown that in general, PRIZ space-time light modulators transform signals nonlinearly." (37:72) Indeed, studies of the PRIZ involve nonlinearities of many forms, or more specifically, the effect of nonlinearities on the accurate and consistent production of optical data. For example, even in our relatively simple one-dimensional models, a system of 300 nonlinear differential equations is used to predict charge distributions within the crystal. Nonlinearities are therefore at the forefront of PRIZ

investigation and development, giving the device its great promise, but simultaneously complicating our understanding of its basic operation.

The primary goal of this thesis is to successfully reproduce and analyze data presented by the Russian scientists A. M. Bliznetsov, Yu. I. Kuz'min, and A. V. Khomenko in their paper, "Investigation of Reciprocity in the PRIZ Space-Time Light Modulator". This paper appeared in the journal Soviet Physics Technical Physics in March 1988. Reference will also be made to self erasure results reported in a previous paper published in the same journal. This earlier paper by A. M. Bliznetsov, V. V. Bryksin, L. I. Korovin, S. V. Miridonov, and A. V. Khomenko entitled, "Injection Mechanism of Dynamic Image Selection in PRIZ Space-Time Light Modulators", was published in July 1987. These papers will be referred to as the 1988 and 1987 papers, respectively.

Before further detailing the goals of this thesis, the reader is reminded that, although the PRIZ derives its properties from the multi-dimensional aspects of the electrooptic effect, one-dimensional modelling is the first step in achieving a basic understanding of the PRIZ. In our one-dimensional model, the ultimate effect we will observe is the distribution of space charge versus time and crystal depth. The space charge density for a given point and time is computed by subtracting the density of conduction electrons (n_e) and ionized, or filled, traps (n_-) from the density of ionized donors (n_+), and multiplying the result by the basic unit of charge, e. In one dimension, we can only analyze charge distributions produced by uniform illumination of the PRIZ face. Such illumination produces a space

charge that can only vary along the longitudinal crystal axis, for any given time. This longitudinally varying space charge modifies the longitudinal electric fields within the crystal. The resulting transverse fields, however, are negligible and no transverse electrooptic effect is observed. In other words, the read light will not be modulated bv a PRIZ under uniform illumination. This restriction severely limits our ability to analyze such effects as reciprocity, self erasure, and regeneration, which emerge as predominantly multi-dimensional effects in this study. Indeed, some well documented experimental effects were not observed at all in our one-dimensional model.

Specifically, this study will use well known electromagnetic formulas and a differential equation solving routine to predict the charge distributions for various intensities and exposures for the DI, SI, and conducting PRIZ. Using this scheme, we will attempt to duplicate the results reported in Figures Three and Four of the 1988 paper. Space charge data will be manipulated to produce information on the longitudinal electric field and current densities within the crystal. This information will be used to validate the authors' assertions about the role of injection currents during various illumination intensities and exposures. We will also analyze the authors' assertions about reciprocity in the PRIZ. Finally, we will investigate the phenomenon of self erasure which is implied in Figure One of the 1988 paper and explicitly studied in Figure One of the 1987 paper. The ultimate goal, of course, is a greater understanding of the

basic mechanisms of the PRIZ. This paper will hopefully exhaust one-dimensional efforts to unravel the PRIZ and provide guidance for further multi-dimensional models.

The following sequence will be followed in this study. First, background information will be presented to include a general description, basic theory, and previous experimental and analytical work. Next, we will discuss the mathematical and computer modelling process. We will then examine the 1987 and 1988 papers in detail and define our specific modelling goals in the context of these papers. Finally, we will attempt to reproduce the experimental and analytical results of the 1988 paper. Where our results differ, we will offer explanations, and where our one-dimensional efforts fall short, we will highlight multi-dimensional studies that should be pursued.

II. Background

General Description

A typical PRIZ consists of a thin slab (approximately one millimeter or less) of BSO with transverse dimensions of 10 mm by 10 mm. The two large flat faces of the crystal are coated with transparent insulators in the case of the DI PRIZ, while only the flat face serving as the cathode contact is insulated for an SI PRIZ. The conducting PRIZ has no insulating layers. Transparent electrodes made from Platinum, InO_2, or another conducting material are deposited over the insulating layers, or directly onto the crystal. These electrodes are connected to a power supply that can provide bias voltages of several kilovolts. The write light can be laser light or incoherent light, and the read light is generally laser light of a much smaller photon energy than the write light. The write light normally consists of an intensity-modulated image that deposits varying amounts of energy over the illuminated face of the crystal. In our one-dimensional models, however, the crystal is uniformly illuminated. Appropriate optical devices are used to direct, focus, and analyze the write and read beams. Figure 1 shows a simplified schematic of a PRIZ device.

Theory

Basic principles from the fields of solid state physics, electromagnetism, and optics are used to understand the PRIZ. When these basics are combined to model PRIZ operation, however, the combined effects are no longer basic, and the macroscopic results are often

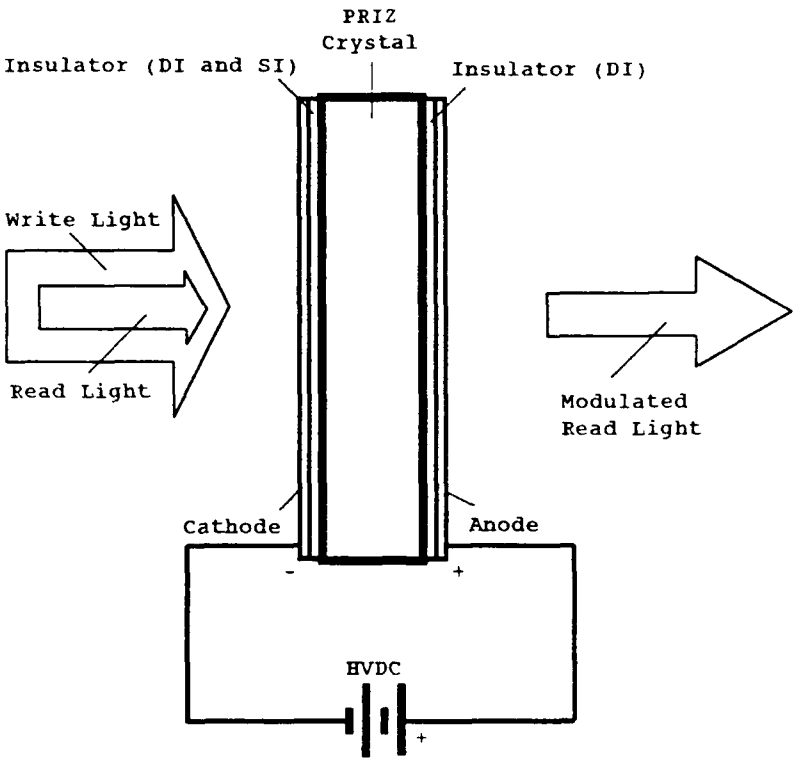

Figure 1. PRIZ Configuration (Side View)

difficult to predict. This section will provide qualitative explanations of the basic physical principles governing the operation of the PRIZ. The mathematical formulas that model these principles will be presented in section III.

The first effect to be studied is photogeneration. This is the process by which donor atoms are ionized by the incident write light, releasing electrons into the conduction band of the PRIZ crystal. The primary parameters involved are donor energy level, density of donors,

write light intensity and frequency (or energy), quantum efficiency, and absorption coefficient. To achieve photogeneration, the energy of the write light must be at least as great as the donor energy level (expressed in units below the conduction band). Given this condition, the probability that a single donor center will be ionized, if illuminated by a photon, is expressed by the quantum efficiency. The quantum efficiency used throughout this report is one, as reported by Sprague for BSO illuminated with light at 441 nm, or 2.6 eV photon energy (Sprague:1677). The number of photoelectrons generated, by light of appropriate energy, will generally increase with increasing values of donor density and write beam intensity. However, since the number of donors is finite, eventually the donors will be depleted and photogeneration will stop. In BSO the donors are Silicon vacancy centers located 2.6 eV below the conduction band. The absorption coefficient characterizes how the light energy is absorbed as it passes through the thickness of the crystal. Light with a large absorption coefficient will be more strongly absorbed in the initial portions of the crystal.

More complicated additional processes exist that affect the formation of a space charge in the PRIZ crystal. For example, Peltier refers to luminescence centers at 1.3 eV and 2.25 eV in BSO that can release or trap conduction electrons (30:3684). Furthermore, we know from solid state physics that the holes, or ionized donor centers, can also drift under the influence of an electric field. The mobility of holes in BSO is reported to be so low, in comparison to the mobility of

conduction electrons, as to be inconsequential in our calculations (14:1488). Most of the additional processes alluded to above are also relatively minor effects, and therefore, are not specifically addressed in our models or the Russian models.

Once the photoelectrons are released into the conduction band, they will drift in the external field produced by the transparent electrodes. The rate of this drift will depend on the strength of the electric field and the electron mobility, a material property. The drift will stop when the electron reaches the anode or when it is captured by a trap site within the crystal. In BSO, these trap sites can be shallow, 0.3 eV to 0.6 eV, or deep, 1.3 eV and 2.25 eV (12:878, 21:9). The deep traps correspond to the luminescence centers mentioned earlier. The rate of trapping will depend on the number of electrons in the conduction band, the density of trap sites, and the trap recombination coefficient. The trap recombination coefficient is a material parameter that reflects specific quantum characteristics of the traps. Like donors, traps are finite in number and can be completely filled. In BSO, the average time between photogeneration and trapping is on the order of 0.1 msec (6:376).

Since the donor and trap sites are considered fixed within the crystal, when donors are ionized and release electrons that drift to trap sites, the result is a net space charge within the volume of the crystal. At any given point within the crystal, the net space charge density can be calculated by subtracting the charge density of free electrons and negatively ionized traps from the charge density of

positively ionized donors. Neglecting further photogeneration (the write light is turned off) and electron injection through the cathode; the only way for an existing space charge to change is through deionization. This can occur through recombination of ionized donors with conduction electrons or through detrapping, in which a trapped electron is thermally or optically excited back into the conduction band. These two processes are dependent upon the donor recombination coefficient and the average ionized trap lifetime, respectively. The donor recombination coefficient is a quantum mechanical parameter that, together with the number of free electrons and number of ionized donors, determines the rate at which the ionized donors will deionize or recombine. The average trap lifetime due to thermal excitation for BSO is very large at standard temperatures. This means that detrapping, or deionization of traps, is a minor effect. Detrapping due to optical excitation by the read light is also a minor effect since the quantum efficiencies involved are very low. This is in spite of the fact that read beam energies are on the order of 2 eV. Figure 2 is a diagram of the energy levels in BSO at room temperature.

The previous paragraph detailed the individual processes by which a space charge is formed in the PRIZ crystal. The formation of this space charge, which varies with position and time, is the basis of PRIZ operation. It is this space charge distribution which modifies the longitudinal electric field within the crystal. In the more general case of nonuniform illumination, the space charge will also produce transverse electric fields within the crystal that modulate the read

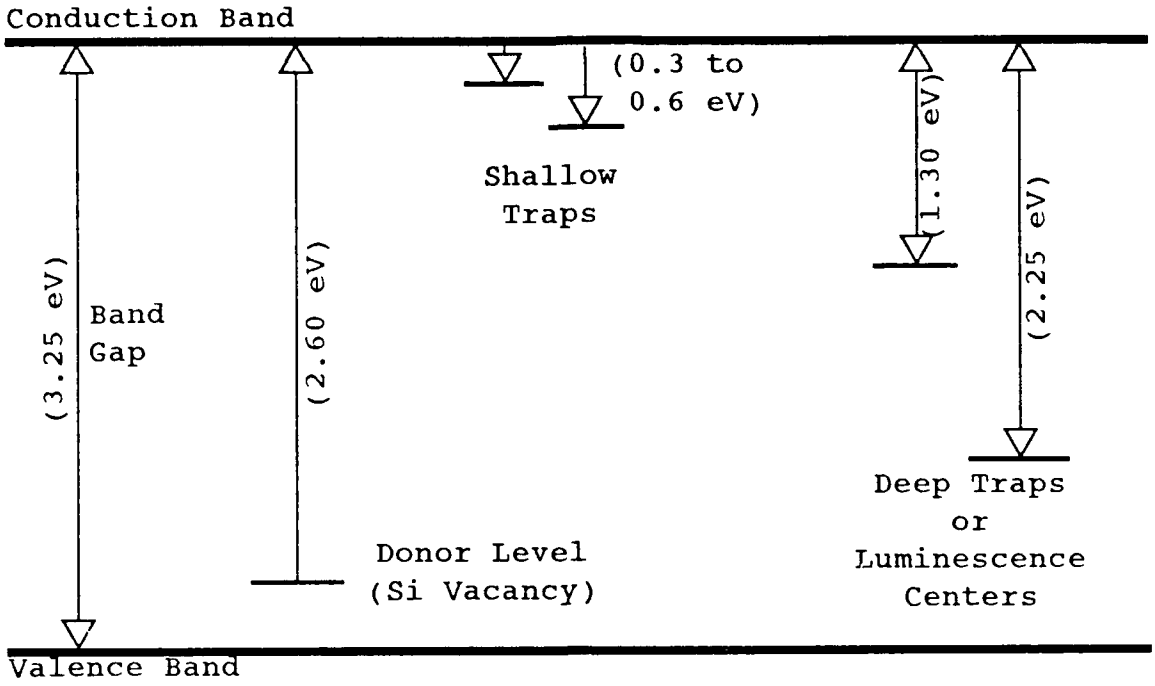

Figure 2. Energy Band Diagram of BSO at Room Temperature

beam through the transverse linear electrooptic, or Pockels, effect, which will be discussed later.

The macroscopic result of space charge formation in time is a very complicated process, however, some general trends can be presented. The most obvious effect is the formation of a net positive space charge region in the body of the crystal next to the negative, illuminated electrode. A negative space charge region is formed near the anode as the photoelectrons drift under the influence of the external electric field and either become trapped or accumulate at the anode. Since no insulator is present on the anode in an SI or conducting PRIZ, the electrons that drift there will be extracted. The resulting

longitudinal charge separation modifies the electric field within the crystal. In the region of the crystal where the net space charge changes from positive to negative, the net electric field will be reduced. As a result, the conduction electrons in this region are slowed and experience enhanced trapping. The enhanced trapping further modifies the net space charge and the net electric field within the crystal. As a result, the region of enhanced trapping moves toward the cathode as photogeneration continues. As the net positive space charge region retreats behind this region of enhanced trapping, the slope of the net space charge distribution curve at the crossover point, or bottleneck, becomes more steep and pronounced (13:33, 32:336). Eventually, the net positive space charge is confined to a very narrow region adjacent to the cathode. The process is modified if injection of electrons is allowed through the negative cathode. This can only occur in the conducting PRIZ, and the specific effects on the space charge are a primary focus of this report. At this point, we can assert, however, that the injection will depend on the material properties of the electrode and the net electric field at the cathode. Also, in the case of uniform illumination, we can expect uniform injection, although the injection will most certainly depend on time.

The PRIZ is actually a refinement on a previous optical storage device called the PROM. PROM is an acronym for Pockels Readout Optical Modulator and refers to an optical device that modulates light according to the longitudinal linear electrooptic (Pockels) effect. This effect occurs when a longitudinal electric field is applied to a suitable

crystal, such as BSO, in an appropriate orientation. The electric field modifies the crystal's index of refraction, producing a fast and a slow axis within the crystal making it birefringent (25:354, 33:816). When light traverses a birefringent crystal, phase changes are induced. Since the originally applied electric field is modified within the crystal when the write light induces a space charge, the birefringence, and subsequent net phase change, is very complex.

The linear electrooptic (Pockels) effect described above is a result of the longitudinal electric field within the PROM crystal. The PRIZ, however, modulates light according to the transverse electrooptic effect. This effect is due to the transverse electric fields produced by the space charge distribution. These transverse fields modulate the read light as it passes through the crystal. The longitudinal fields do not contribute a net modulation to the light (31:823, 32:330, 37:68).

The PRIZ and PROM devices are similar in geometry and method of operation, however, the differences in modulation mentioned above are produced by different crystal orientations. As stated by Gardner and Luke, "PROM devices use a (100) crystal orientation in which the [100] direction is normal to the sandwich structure. PRIZ devices use either (111) or (110) orientations with the corresponding direction normal to the sandwich structure." (23:19) The sandwich structure refers to the crystal at the center, with dielectric insulators on either side (for a DI PRIZ), and transparent electrodes over both insulators. Therefore, through selective orientation, either the longitudinal or transverse electrooptic effect can be highlighted. In addition to BSO, other

suitable crystals are produced from Bismuth Titanate ($Bi_{12}TiO_{20}$), Bismuth Germanate ($Bi_{12}GeO_{20}$), Lithium Niobate ($LiNbO_3$), and numerous other compounds (17:757). Specific modulation of a suitable crystal will depend on individual material properties such as electron mobility, donor energy level and density, density of traps, crystal symmetry, and electrooptic coefficients. In this report, we will deal exclusively with BSO even though more efficient crystals have been developed and studied (34:107). It is interesting to note, once again, that uniform illumination will not produce significant transverse electric fields within the PRIZ crystal, and therefore, the transverse electrooptic effect will not be observed (20:3849). This highlights a limitation of the one-dimensional study offered here.

Previous Work

Much of the analytical and experimental work on the PRIZ has been conducted in the Soviet Union. Bryksin, Petrov, Bliznetsov, Khomenko, Shlyagin, and Astratov have published numerous reports on the PRIZ. Much of AFIT's work, to include this thesis, have concentrated on experimentally or analytically reproducing Soviet results. These efforts have met with overall success as reported by Shields, Nilius, Cushing, Gardner, and Nelson (36:1, 29:1, 21:1, 22:1, 28:1). Anderson provided pioneering work on specific aspects of PRIZ crystal damage, due to high internal fields, in his 1986 AFIT thesis (1:1). Luke and Gardner quantify the threshold energy density for damage at 1.0 mJ/cm^2 (23:21). This experimentally derived damage threshold should be kept in mind throughout this analytical study, as we, and the Russians, are

often dealing with exposure energy densities well above these values. Our analytical solutions do not model the catastrophic failures that experimentally occur.

The Russian articles leading up to the 1987 and 1988 papers studied in this report show varying degrees of sophistication and accuracy. Some papers offer gross approximations that are surprisingly accurate in some operating regimes. For example, Bryksin neglects trapping altogether in a 1984 paper, and again in a 1986 paper offering an "exact solution" for the photoinduced charge in photorefractive crystals (10:2195, 9:80). Similarly, Bryksin and others frequently ignore the absorption coefficient, and assume that the write beam is absorbed totally in a certain crystal thickness near the cathode (14:1488). Other parameters that may or may not be considered are depletion of donors, filling of traps, thermal ionization of traps, recombination of donors, diffusion current, and injection. As should be evident, one of our major problems was the uncertainty as to what approximations the Russians used in the particular papers we studied. This, coupled with imperfect translation, made thorough detective work as invaluable as mathematical and physical rigor.

III. Mathematical and Computer Modelling

As previously discussed, the mathematical models, and subsequent computer models, used depend upon the approximations made. With this in mind, we have developed two distinct master models from which all minor variations are applied. The first master model is comprehensive and gleans the best modelling information from the entire body of previous Russian and AFIT work on the PRIZ. Few effects are neglected in this model although some effects are numerically insignificant in most operating regimes. For example, depletion of donors is modelled even though Bryksin reports that depletion of donors has never been observed (18:2052). Likewise, thermal ionization of traps is modelled even though the characteristic time for this event is several orders of magnitude greater than most PRIZ exposure times.

The second master model, or clipped model, only models those effects that are explicitly mentioned in the 1988 paper by Bliznetsov, et al. These are trapping, depletion of donors, absorption length modelling for the write beam, and cathode field-dependent injection (6:374). All models used in this study will be based on one of the two master models presented above. Minor deviations from the standard models will be highlighted.

Rate Equations

Each of the master models consists of three basic rate equations. These are the net rate of production of ionized donors, the net rate of production of ionized traps, and the time rate of change of free

electrons in the conduction band of the crystal. When these equations, with appropriate initial and boundary conditions, are applied to a specific location in the crystal at a specific time, the number of ionized donors, ionized traps, and free electrons can be calculated. The determination of appropriate boundary conditions is nontrivial since each region's boundary conditions are dependent on the other regions' boundary conditions. With this information, however, the net space charge density can be calculated along with the net electric field and current density for that particular region of the crystal. The same three equations with different initial and boundary conditions can also be used to compute the net space charge density in the other regions of the crystal. The macroscopic result is an overall view of the net space charge density, net electric field, and current density for the entire crystal. The space charge distribution will evolve in time according to the rate equations, and the overall result can be used to predict the longitudinal and transverse fields that lead to the longitudinal electrooptic effect (PROM) and the transverse electrooptic effect (PRIZ). Accepting the rate equations as valid mathematical representations of the physical processes within the PRIZ, the accuracy of the results will depend on the accuracy of the material parameters entered in the equations, the bin size, and the tolerance of the differential equation solving technique used. The bin size is the fractional slice of the crystal over which the rate equations are applied. Bin size will be discussed in detail in a later subsection.

The first rate equation is the net rate of donor ionization. For master model one, this equation models exponential absorption of light using the absorption coefficient, depletion of donors, and recombination of donors. The corresponding rate equation for the clipped master model does not include the recombination of donors term. Eqs (1) and (2) below give the net donor ionization rate equations for master models one and two, respectively:

$$\frac{\partial n_+'}{\partial t'} = G'(N_d' - n_+') - \frac{n_e' n_+'}{\zeta_d'} \tag{1}$$

$$\frac{\partial n_+'}{\partial t'} = G'(N_d' - n_+') \tag{2}$$

where

n_+' = density of ionized donors (cm^{-3})
t' = time (sec)
G' = generation rate (sec^{-1})
N_d' = density of donors (cm^{-3})
n_e' = density of free electrons (cm^{-3})
ζ_d' = donor recombination coefficient (sec/cm^3)

The prime notation (′) for the variables given above denotes dimensional variables that will undergo normalization. The generation rate, G′, given above is dependent on numerous variables as described in section II. Equation (3) on the following page gives the mathematical formulation for G′, where we have introduced a new parameter called the generation coefficient, g′:

$$G' = \frac{I'\eta}{h\nu'}\frac{\alpha'}{N_d'}\exp(-\alpha' z') = g'\frac{\alpha'}{N_d'}\exp(-\alpha' z') \qquad (3)$$

where

I' = write light intensity (Watts/cm^2)
η = quantum efficiency
h = Planck's constant (J•sec)
ν' = write light frequency (Hz)
α' = absorption coefficient (cm^{-1})
z' = longitudinal crystal depth (cm)
g' = generation coefficient (cm^{-2}sec^{-1})

Equation (3) is consistent with Russian models of the generation rate (8:1529). The generation coefficient, g', is the parameter that is usually referenced instead of the generation rate, G'.

The second rate equation is the net ionization of traps, or more simply, the net trapping. For master model one, this equation models the rate of trapping, filling of traps, and deionization of traps. The corresponding equation for the clipped master model two does not model the filling of traps or the deionization of traps. Equations (4) and (5) give the net ionization of traps rate equations for master models one and two, respectively:

$$\frac{\partial n_-'}{\partial t'} = n_e'\frac{(N_t' - n_-')}{\zeta_t'} - \frac{n_-'}{\tau_t'} \qquad (4)$$

$$\frac{\partial n_-'}{\partial t'} = \frac{n_e'}{\tau_d'} \qquad (5)$$

where

n_-' = density of ionized traps (cm^{-3})
N_t' = density of traps (cm^{-3})
ζ_t' = trap recombination coefficient (sec/cm^3)
τ_t' = average ionized trap lifetime (sec)
τ_d' = average electron drift time before trapping (sec)

Equation (5) for the second, or clipped, model is the more common form in most Russian publications (8:1528, 12:879).

The final rate equation models the time rate of change of free electrons in the conduction band of the crystal. This equation is derived from electromagnetic principles which, although basic, are worth repeating here to highlight approximations. We start with two of Maxwell's equations given in Eqs (6) and (7) below:

$$\nabla \cdot \bar{D}' = \nabla \cdot \epsilon \bar{E}' = \rho' \tag{6}$$

$$\nabla \times \bar{H}' = \bar{J}_t' = \bar{J}_c' + \bar{J}_d' + \bar{J}_{diff}' \tag{7}$$

The "t", "c", "d", and "diff" subscripts on the current density terms, $\bar{J}'$, refer to total, conduction, displacement, and diffusion currents, respectively. At this point, approximations are made for the total current. In some papers, Bryksin and others ignore everything except conduction current (9:80). In most works, however, only the diffusion current is neglected. We will neglect diffusion current in both our master models while keeping both conduction and displacement current. Bryksin addresses the validity of this approximation in one of his 1984

papers (14:1491). Under most conditions, the effects of diffusion current are negligible.

The development of the final rate equation continues in Eqs (8) to (11) below. Equation (8) is simply the del dot product of both sides of Eq (7), with total current approximated by conduction current and displacement current:

$$\nabla \cdot \nabla \mathbf{X} \bar{H}' = 0 = \nabla \cdot \bar{J}_t' = \nabla \cdot (\bar{J}_c' + \bar{J}_d') \tag{8}$$

$$\nabla \cdot (\bar{J}_c' + \frac{\partial \bar{D}'}{\partial t'}) = 0 \tag{9}$$

$$\frac{\partial}{\partial t'}(\nabla \cdot \bar{D}') + \nabla \cdot \bar{J}_c' = 0 \tag{10}$$

$$\frac{\partial \rho'}{\partial t'} = -\nabla \cdot \bar{J}_c' = -\frac{\partial \bar{J}_c'}{\partial z'} \tag{11}$$

Equation (11) has used Eq (6) and the fact that the divergence in our one-dimensional models reduces to a partial derivative with respect to the longitudinal dimension of the crystal. The last two relationships needed to complete the development are given in Eqs (12) and (13) on the following page:

$$\bar{J}_c' = e\mu n_e' \bar{E}' \tag{12}$$

$$\rho' = e(n_+' - n_-' - n_e') \tag{13}$$

where

e = elementary charge ($1.6022 \cdot 10^{-19}$ C)
μ = mobility of electrons ($cm^2/V \cdot sec$)

Substituting Eqs (12) and (13) into Eq (11) and rearranging we arrive at the final form for the third rate equation. Since we will only be dealing in one dimen' , the vector notation will be omitted for the rest of the repo1. Equation (14) below, therefore, models the time rate of chan;e of free electrons in the conduction band:

$$\frac{\partial n_e'}{\partial t'} = \frac{\partial n_+'}{\partial t'} - \frac{\partial n_-'}{\partial t'} + \frac{\partial}{\partial z'}(\mu n_e' E') \tag{14}$$

Equation (14) is valid for both master models. When the appropriate equations for the first two terms on the right hand side of Eq (14) are substituted, however, the resulting equations for the two master models become different.

To summarize, the three rate equations for the comprehensive master model one are Eqs (1), (4), and (14). The corresponding rate equations for the clipped master model two are (2), (5), and (14).

Normalization

Equations given in the previous section were dimensional. To facilitate further mathematical and computer calculations, all variables were undimensionalized, or normalized. The normalization we used is based on the initial transient time, t_0', which is derived from the crystal thickness, d_0', the electron mobility in the crystal, μ, and the voltage applied to the transparent electrodes, V_0'. In this report, the initial transient time will also be referred to as the time constant. The initial transient time is simply the time required for a free electron to drift from the cathode to the anode through the crystal under the influence of the applied electric field, assuming no trapping and no recombination with holes. This normalization is fairly standard, however, others are used. For example, Bryksin normalizes to "the characteristic time for electron trapping by a trap" in one of his 1983 papers (7:686). The "characteristic time for electron trapping" corresponds to τ_d in Eq (5) on page 22. The normalization most frequently used in Russian papers, including those by Bryksin, is identical to the normalization presented in this paper. Table 1 on the next page details the normalization factors and subsequent normalized variables. Dimensional parameters such as e, h, ϵ, and μ, that represent well known physical constants or material parameters, do not carry the dimensional (') notation despite the fact that they are dimensional. Furthermore, some variables such as I' and $\mathcal{E}'$ are never explicitly normalized individually.

Table 1

Normalization Factors and Normalized Variables

NORMALIZATION FACTORS	DESCRIPTION
d_0'	Device thickness (cm)
$t_0' = d_0'^2/(\mu V_0')$	Initial transient time (sec)
$n_0' = \epsilon V_0'/(e d_0'^2 \cdot 10^2)^*$	Concentration normalization factor (cm^{-3})
$\mathscr{E}'$	Total exposure energy (J/cm^2)
I'	Write light intensity (W/cm^2)
V_0'	Applied external voltage (Volts)
μ	Mobility of electrons ($cm^2/V \cdot sec$)
$\epsilon = \epsilon_r \epsilon_0$	Permittivity (F/m)
ϵ_r	Relative Permittivity
$\epsilon_0 = 8.8542 \cdot 10^{-12}$	Permittivity of free space (F/m)
$e = 1.6022 \cdot 10^{-19}$	Elementary charge (C)

* Factor of 10^2 in n_0' is a conversion factor to account for the difference in length units between ϵ and d_0'.

NORMALIZED VARIABLES	DESCRIPTION
$n_+ = n_+'/n_0'$	Density of ionized donors
$n_- = n_-'/n_0'$	Density of ionized, or filled, traps
$n_e = n_e'/n_0'$	Density of free electrons
$n_s = n_s'/n_0'$	Injection coefficient of cathode
$N_d = N_d'/n_0'$	Density of donors
$N_t = N_t'/n_0'$	Density of traps
$t = t'/t_0'$	Time
$t_{exp} = \mathscr{E}'/(I' t_0')$	Exposure time
$\tau_t = \tau_t'/t_0'$	Average ionized trap lifetime
$\tau_d = \tau_d'/t_0'$	Average electron drift time
$z = z'/d_0'$	Longitudinal distance or crystal depth
$\rho = \rho'/(e n_0')$	Charge density
$\alpha = \alpha' d_0'$	Absorption coefficient
$E = E'/(V_0'/d_0')$	Electric field intensity
$J = J'/(e n_0' d_0'/t_0')$	Current density (J_t, J_c, J_d, or J_{diff})
$\zeta_d = \zeta_d'/(n_0' t_0')$	Donor recombination coefficient
$\zeta_t = \zeta_t'/(n_0' t_0')$	Trap recombination coefficient
$G = G' t_0'$	Generation rate
$g = g'/(n_0' d_0'/t_0')$	Generation coefficient

After normalization, the three rate equations for master model one become

$$\frac{\partial n_+}{\partial t} = g\frac{\alpha}{N_d}(N_d - n_+)\exp(-\alpha z) - \frac{n_e n_+}{\zeta_d} \tag{15}$$

$$\frac{\partial n_-}{\partial t} = n_e\frac{(N_t - n_-)}{\zeta_t} - \frac{n_-}{\tau_t} \tag{16}$$

$$\frac{\partial n_e}{\partial t} = \frac{\partial n_+}{\partial t} - \frac{\partial n_-}{\partial t} + \frac{\partial}{\partial z}(n_e E) \tag{17}$$

Similarly, the normalized rate equations for the clipped master model two are

$$\frac{\partial n_+}{\partial t} = g\frac{\alpha}{N_d}(N_d - n_+)\exp(-\alpha z) \tag{18}$$

$$\frac{\partial n_-}{\partial t} = \frac{n_e}{\tau_d} \tag{19}$$

$$\frac{\partial n_e}{\partial t} = \frac{\partial n_+}{\partial t} - \frac{\partial n_-}{\partial t} + \frac{\partial}{\partial z}(n_e E) \tag{17}$$

Computer Modelling

Before the rate equations can be solved numerically with a finite difference scheme, they must be converted to a discrete form and initial and boundary conditions must be specified. To accomplish this, the crystal is divided longitudinally into 100 discrete and equal bins. Accuracy will improve, of course, with an increased number of bins. Our differential equation solver software, Mathlib DEQSOLVE by Innosoft International, Inc., would accept up to 200 bins. The Russians apparently used 201 bins (8:1530).

The time step over which a solution is attempted must also be specified. The magnitude of the time step was manipulated by specifying an absolute tolerance value to the differential equation solver software. The software then internally determined the appropriate time step to ensure the absolute tolerance value was not exceeded. Early on, we determined that an absolute tolerance value of 10^{-7} resulted in excessive computation times and did not significantly improve accuracy. As a result, a tolerance value of 10^{-2} was used for most runs. The Russians use a finite difference scheme with FORTRAN EC. The specifics of the program are not provided, however, they profess an accuracy better than 10^{-3} in previous reports (8:1530).

Since the discrete nature of the time step was made transparent to the user by the software, the first two rate equations are inherently discrete and require only minor modifications in order to be acceptable to the software. The third rate equation, however, had to be modified as follows:

$$\frac{\Delta n_e}{\Delta t} = \frac{\Delta n_+}{\Delta t} - \frac{\Delta n_-}{\Delta t} + \frac{\Delta (n_e E)}{\Delta z} \tag{20}$$

Using secondary subscripts to denote the bin number and the fact that, after normalization, $1/\Delta z$ equals nbin, the last term in Eq (20) is more conveniently expressed by

$$\frac{\Delta (n_e E)}{\Delta z} = (n_{ej} E_j - n_{e(j-1)} E_{(j-1)}) nbin \tag{21}$$

After the rate equations have been made discrete and appropriate parameters entered, the solution can proceed. The initial values for density of ionized donors, ionized traps, and free electrons are set to zero, and cathode and anode boundary conditions, appropriate to the type of PRIZ, are entered. For the DI and SI PRIZ, the boundary value for n_{e0} is set to zero since no injection is allowed through the cathode. For the conducting PRIZ, the value of n_{e0} must reflect injection. To accomplish this, we have used the same model as Bliznetsov reports in the 1988 paper (6:375). The dimensional form for this equation is actually specified by Bliznetsov, however, normalization does not change the equation's form as can be seen by Eq (22) on the next page:

$$n_{e0}(t) = n_s\left[1 - \frac{E_0(0)}{E_0(t)}\right] \tag{22}$$

where

$n_{e0}(t)$ = electron density at the cathode at time t
n_s = cathode injection coefficient
$E_0(0)$ = electric field at cathode at time 0
$E_0(t)$ = electric field at cathode at time t

The value of n_e at the anode, or n_{e100}, is automatically calculated by the routine. For a DI PRIZ, however, the term $n_{e100}E_{100}(t) = J_{c100}$ is set to zero since there can be no current through the anode. The various values for $E_0(t)$, the cathode field, and $E_j(t)$, where the subscript j refers to the bin number, are calculated with Eqs (23) and (24) below:

$$E_0(t) = -1 + \left(\frac{1}{nbin}\right)^2 \sum_{j=1}^{nbin} (j - nbin)(n_{+j} - n_{-j} - n_{ej}) \tag{23}$$

$$E_j(t) = E_0(t) + \left(\frac{1}{nbin}\right) \sum_{k=1}^{j} (n_{+k} - n_{-k} - n_{ek}) \tag{24}$$

Equations (23) and (24) are derived from manipulations of the discrete form of Eq (6). The derivation of Eqs (23) and (24) forces the integral of the electric field across the length of the device to equal $-V_0$ for

all time. The validity of the derivation is tested during all calculations by simultaneously calculating the net accumulated charge density within the crystal as time progresses. A DI PRIZ will always have a zero net accumulated charge density, since no charges can enter or leave the crystal, however, the SI and conducting PRIZ will develop a net charge over time.

The only parameter that remains to be specified is the exposure time. The exposure time must be entered in normalized time units according to Eq (25):

$$t_{exp} = \frac{\mathscr{E}'}{I' t_0'} \tag{25}$$

where

t_{exp} = normalized exposure time
$\mathscr{E}'$ = total exposure energy (J/cm^2)
I' = write light intensity (Watts/cm^2)

Given appropriate entries for all the parameters specified in the paragraphs above, the software will compute ionized donor density, ionized trap density, and free electron density versus time and distance. Using this information, the net charge density can be computed, as well as the internal electric field and current density, versus position and time. The computation time for one run is anywhere from 15 minutes to several hours depending on exposure time, write light intensity, and numerous other factors. For example, since the number of differential equations that must be solved for each time step is nbin times three, the computation times increase with an increase in nbin.

IV. Detailed Analysis of Soviet Journal Articles

Discussion and Interpretation

The two Soviet papers we specifically address in this thesis are "Investigation of Reciprocity in the PRIZ Space-Time Light Modulator", by Bliznetsov, Kuz'min, and Khomenko (1988 paper) and "Injection Mechanism of Dynamic Image Selection in PRIZ Space-Time Light Modulators", by Bliznetsov, Bryksin, Korovin, Miridonov, and Khomenko (1987 paper). Most of our information on Soviet analytical modelling techniques is derived from previous works by Bryksin. Bryksin is referenced in the 1987 and 1988 papers, as are Petrov, Shlyagin, Astratov, and others. Bliznetsov does not appear as an author in any of the additional references we have used. His work on the conducting PRIZ appears to be limited to the 1987 and 1988 papers, and the extent to which he has chosen unique nomenclature or modelling techniques is unclear. Both papers contain data that is not fully specified and subject to some interpretation. The experimental data presented in both papers is especially nebulous and, as a result, we experienced greater success in modelling the Russian's analytical data than their experimental data. Even the Russians, however, claim to analytically model only the "qualitative" aspects of their own experimental data (6:374).

In the 1988 paper, the authors initially present experimental data for the operation of a conducting PRIZ over the range of writing light intensities from 30 $\mu W/cm^2$ to 300 mW/cm^2. Their PRIZ consists of a

0.45 mm thick $Bi_{12}SiO_{20}$ (BSO) crystal, with electrodes biased by a two kilovolt DC power supply. The image, a 20 μm wide strip, is written with a helium-cadmium laser (λ = 441 nm). The imaged strip produces transverse electric fields within the PRIZ, and a subsequent response. The image is read with a helium-neon laser (λ = 633 nm) with an intensity of 10 $\mu W/cm^2$.

As a basis for our interpretation, we assumed that the response measured, and experimentally reported, by the Russians was the instantaneous output, or throughput, of the read light for a given condition of exposure. In other words, no time delay was used to measure the response of the PRIZ to an applied stimulus. The impact of time delay on response will be covered in detail in subsequent sections. At this point, we will simply mention that the finite time required for photogenerated electrons to drift under the influence of the electric field within the crystal results in a delay of response to a given stimulus. Data can be collected by either allowing for or ignoring this delay. We believe rather confidently that the Russians have chosen the latter option. Furthermore, at some point, we must link the results from our one dimensional analytical model to the response data from the multidimensional experiments. The Russians never attempted this, and instead, relied on qualitative explanations to link their experimental and analytical data. Using these qualitative explanations, we attempted to quantify the response produced by our various one dimensional charge distributions. This consisted of predicting the response produced when a one-dimensional charge distribution is placed adjacent to a net zero

charge distribution, resulting in transverse electric fields that modulate the read light. The criterion we chose to quantify the transverse fields is crude, yet consistent with qualitative explanations. We will elaborate on the details of our criterion later in this section. With these overriding assumptions in mind, we continue with our detailed analysis of the Russian papers.

First, the authors experimentally establish a region over which the principle of reciprocity holds. The principle of reciprocity asserts that the response of the PRIZ is independent of write light intensity for a given exposure, where the exposure is given by the product of the write light intensity and time of illumination. They define response somewhat ambiguously as "the total intensity $\mathfrak{R}$ of the readout image at various reading-light intensities." (6:374) The term "reading-light intensities" is certainly intended to be writing-light intensities, however, further interpretation of their definition is difficult. Equation (26) expresses the principle of reciprocity, as reported in the 1988 paper, for values of exposure less than 20 $\mu J/cm^2$:

$$\mathfrak{R} \propto \mathscr{E}' = I' t_{exp}' \tag{26}$$

where

$\mathfrak{R}$ = PRIZ response
$\mathscr{E}'$ = exposure (J/cm^2)
I' = write light intensity (W/cm^2)
t_{exp}' = exposure time (sec)

Figure 3, below, approximates experimental data, presented in Figure One of the 1988 paper, backing up the authors' claims concerning reciprocity. Specifically, we can see from Figure 3 that there is a region where the different intensity curves coincide, indicating reciprocity. We can also see that outside this reciprocity region, for a given exposure, the higher intensity curve produces a higher peak response. Furthermore, we can see that the peak response ($\mathfrak{R}_{max}$) occurs at higher exposures ($\mathscr{E}_{max}$) for higher intensities. Unfortunately, the original graph (Figure One, 1988 Paper) is devoid of any numerical data and we can not be sure what intensities have been drawn. Despite this, the authors' assert, "As shown schematically in Fig. One, at low exposures ($\mathscr{E} \leq 20\ \mu J/cm^2$) the functions $\mathfrak{R}(\mathscr{E})$ coincide to within 30% for all values of the writing-light intensity in the range from $3 \cdot 10^{-5}$ to $3 \cdot 10^{-1}\ W/cm^2$." (6:374) "Fig. One" referred to above is our Figure 3. The authors present a wealth of information on the trends in $\mathfrak{R}_{max}$ and $\mathscr{E}_{max}$. This information is reproduced in Figure 4.

Having provided experimental data on reciprocity, the authors proceed to explain why reciprocity holds below a certain value ($< 20\ \mu J/cm^2$) and fails above this value. In developing their explanation, they assert that the response of the PRIZ is due to the formation of a positive space charge near the cathode. The magnitude and extent of this space charge is determined by two competing factors. The first factor is the photoionization of donors near the cathode, producing electrons that drift toward the anode due to the electric field. This effect increases the positive space charge near the

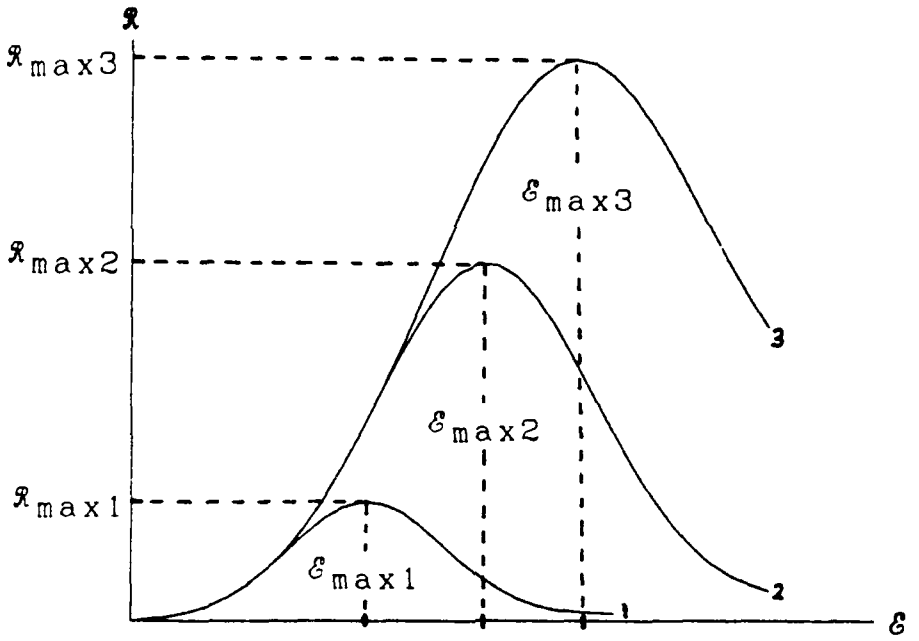

Figure 3. Typical Dependencies of the Intensity ℜ of the Readout Image on the Exposure Energy ℰ for Various Intensities I′ of the Writing Light: I′(1) << I′(2) << I′(3). Taken from Figure 1, 88 Paper (6:374)

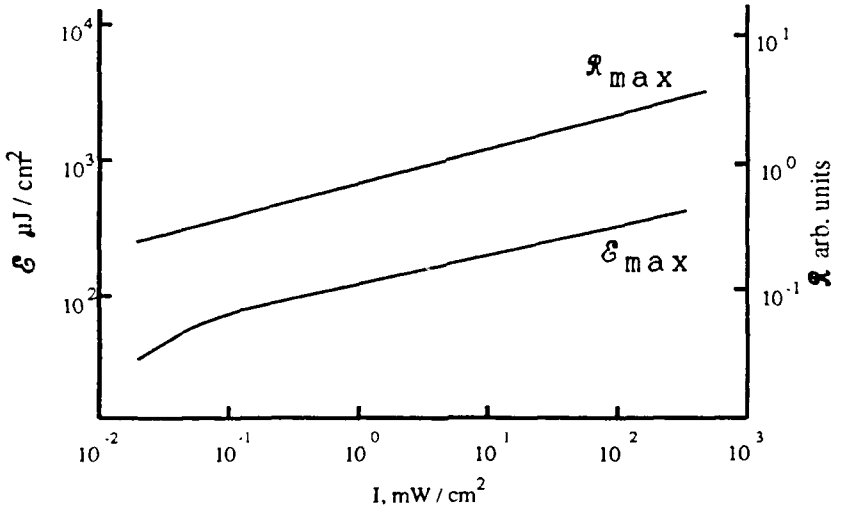

Figure 4. Experimental Dependencies of the Maximum Intensity $\Re_{max}$ of the Readout Image and the Corresponding Exposure Energy $\mathscr{E}_{max}$ on the Writing-Light Intensity I′. Taken from Figure 2, 88 Paper (6:375)

cathode. The second factor is the injection of electrons through the cathode. As previously discussed, the injection of electrons will increase as the cathode electric field increases (becomes more negative). The injection of electrons tends to reduce the positive space charge near the cathode. The authors use the interaction of these two competing factors to explain both the reciprocal and nonreciprocal regions.

To explain reciprocity, the authors state, "In the initial stage of the writing, when the charge density is low, the injection current is low in comparison with the photocurrent and does not have any appreciable effect on the charge accumulation." (6:374) The sentences in the 1988 paper preceding the one above imply that this statement only applies under high intensity conditions. For high intensities and low exposures, the total exposure time corresponds to the "initial stage" mentioned above. Injection, therefore, is not as great a factor at high intensities, and low exposures, as it is for low intensities. As we will soon see, for intensities of $500mW/cm^2$, and exposure values within the reciprocity region, injection is virtually nonexistent. This occurs because the characteristic exposure times, t_{exp}, at high intensities and low exposures, are less than the drift time of the photoelectrons. As a result, the space charge within the crystal can not fully develop and the cathode field remains near its initial value, allowing little injection. At low intensity and low exposure, the characteristic exposure times are long enough to allow significant injection. Presumably, the relative lack of injection at high intensities and low

exposures explains why the response of the PRIZ is reciprocal at exposures less than 20 $\mu J/cm^2$. The preceding explanation is unsatisfying, as it intuitively appears to argue against, rather than for, reciprocity at low exposures. In other words, at low intensity and low exposure, the buildup of positive space charge near the cathode is counteracted to some degree by injection. At high intensity and the same low exposure, however, the buildup of positive space charge near the cathode proceeds unimpeded by injection. If response is indeed due to the density of positive space charge near the cathode, as the authors assert, then the higher intensity light should result in a greater net positive space charge and, therefore, a higher response.

The authors' explanation for the failure of reciprocity at higher exposures is a little more satisfying, even though it seems to be inconsistent with their previous explanation for the existence of reciprocity at low exposures. In their words, "the main factor determining the deviation from the reciprocity law for the PRIZ modulator is the injection of electrons through the contact, which causes the photoinduced positive charge to be partially compensated." (6:376). As we have already seen, they use a very similar argument to explain the reciprocity region at low exposures. Another statement the authors make, in explaining the failure of reciprocity, serves as the basis for our attempts to explain, in one dimension, an essentially two-dimensional process. Again, in their words, "Since an increase in the density of positive charge brings about an increase in the amplitude of modulation of the reading light, the maximum intensity $\mathfrak{R}_{max}$ of the

readout image increases at high intensities of the writing light." (6:374) Here, the authors have connected their unspecified response ($\Re$) to a parameter we can easily model in one dimension, the positive charge density. This connection forms the basis for our efforts to unravel the apparent inconsistencies in the 1988 paper concerning reciprocity.

Next, the 1988 paper mentions a mathematical model for the SI and conducting PRIZ that the authors assert will verify the "qualitative explanations" given for reciprocity (6:374). The model is said to be developed from three previous works by Bryksin, which we also used in our models. Unfortunately, the three Bryksin references were not consistent. One of the references did not model trapping at all, and another neglected displacement current in the formula for total current, presumably in addition to neglecting diffusion current. Furthermore, one of the references models recombination of donors and detrapping while the others do not. In the 1988 paper's model, the authors specifically claim to take into account the ionization and depletion of donors, the trapping of electrons, the decreasing intensity of light versus depth of penetration (absorption coefficient modelling), and the injection of electrons through the cathode at a rate dependent upon the electric field at the cathode. The authors never provide the equations for their entire model, although they do specify the form for the injection as previously specified in Eq (22). The only hint they give as to most of the specific material parameters they use is that the values "corresponded to the conditions of the experiment." (6:374)

The Russians first use their model to compare the net space charge density in an SI and conducting PRIZ under low intensity illumination conditions ($I' = 50\ \mu W/cm^2$). They plot data for net space charge density, ρ, versus longitudinal distance, z', for exposures of 0.4, 2, and 4 $\mu J/cm^2$. Interestingly, they do not report any data for exposures outside the established reciprocity region. This would seem to be a logical step if they are trying to analytically establish injection as the cause for the failure of reciprocity at higher exposures. Even more mysteriously, some of their data appears to show that reciprocity analytically fails where it experimentally succeeded. Figures 5 and 6 are normalized reproductions of their plots for the SI and conducting PRIZ, respectively. Though the graphs appear similar, a quick glimpse at the scales will show that the conducting PRIZ produces net positive space charges that are less than half as high and wide as the corresponding values for the SI PRIZ. As predicted earlier, at low intensity and low exposure, injection reduces the positive space charge region. As they state, "at low writing-light intensities injection of electrons from the contact appreciably reduces both the density of the positive charge and the thickness of the layer that it occupies in the crystal." They further state, "Injection under these conditions thus decreases the magnitude of the STLM response." (6:375) STLM is an acronym for space-time light modulator. With Figures 5 and 6, the authors have established that injection is significant at low intensities, for exposures in the reciprocity region. If they can subsequently show that injection is insignificant at high intensities,

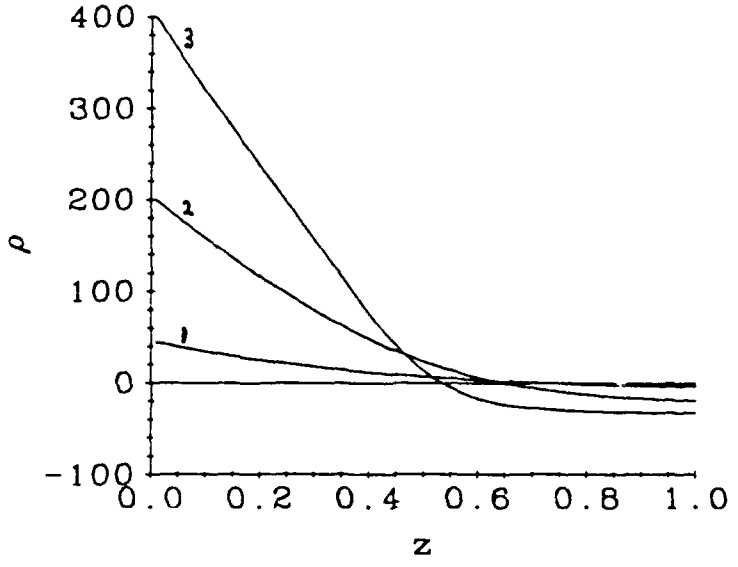

Figure 5. Net Space Charge Density, ρ, versus z for an SI PRIZ with $I' = 50\ \mu W/cm^2$, $\mathcal{E}' = 0.4$ (1), 2 (2), and 4 $\mu J/cm^2$ (3). Taken from Figure 3a, 88 Paper (6:375)

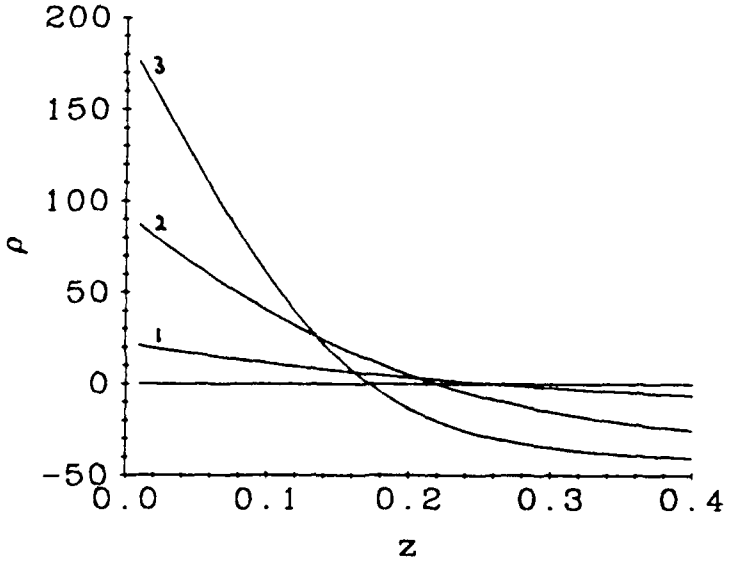

Figure 6. Net Space Charge Density, ρ, versus z for a conducting PRIZ with $n_s = 0.1$, $I' = 50\ \mu W/cm^2$, $\mathcal{E}' = 0.4$ (1), 2 (2), and 4 $\mu J/cm^2$ (3). Taken from Figure 3b, 88 Paper (6:375)

for exposures within the reciprocity region, then some of their earlier claims are justified even though reciprocity is still not clearly established. To fully demonstrate reciprocity, we must plot net space charge densities for the conducting PRIZ at various intensities and exposures, within and without the region of reciprocity. A comparison of conducting PRIZ reciprocity data with SI PRIZ reciprocity data should also serve to highlight the specific effects of injection on reciprocity.

Next, the Russians present data for a conducting PRIZ under high write light intensity ($I' = 500$ mW/cm^2) for exposures of 4, 8, 12, and 24 μJ/cm^2. Again, a seemingly strange choice has been made, as the intensities are well outside the experimental data, and the exposures are all less than or comparable to the reciprocity region boundary. The Soviet data is presented in normalized form in Figure 7. The authors assert that, "As the intensity of the writing light increases, the range of exposures at which injection has only insignificant effect becomes broader." (6:375) Though the data is absent, the authors reinforce the assertion above by stating that the SI PRIZ data for 500 mW/cm^2 differs by less than one percent. If this is true, then the basis for some of the authors' claims, as described in the previous paragraphs, is established. Still, however, no direct comparison is done for space charge densities at various intensities for specific exposure values. One comparison is possible by plotting the 4 μJ/cm^2 exposure curves from Figures 6 and 7 on the same chart. The result of this exercise is shown in Figure 8. The two space charge densities in this plot are

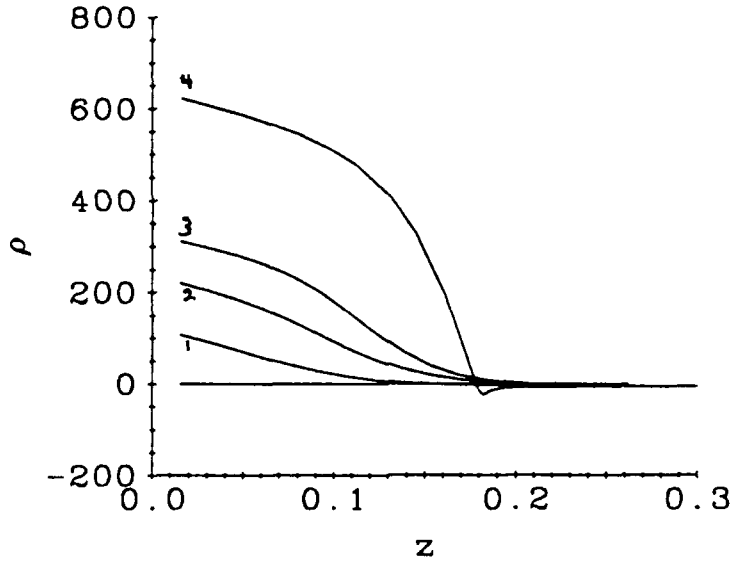

Figure 7. Net Space Charge Density, ρ, versus z for a Conducting PRIZ with n_s = 0.1, I′ = 500 mW/cm^2, $\mathscr{E}$ = 4 (1), 8 (2), 12 (3), and 24 μJ/cm^2 (4). Taken from Figure 4, 88 Paper (6:375)

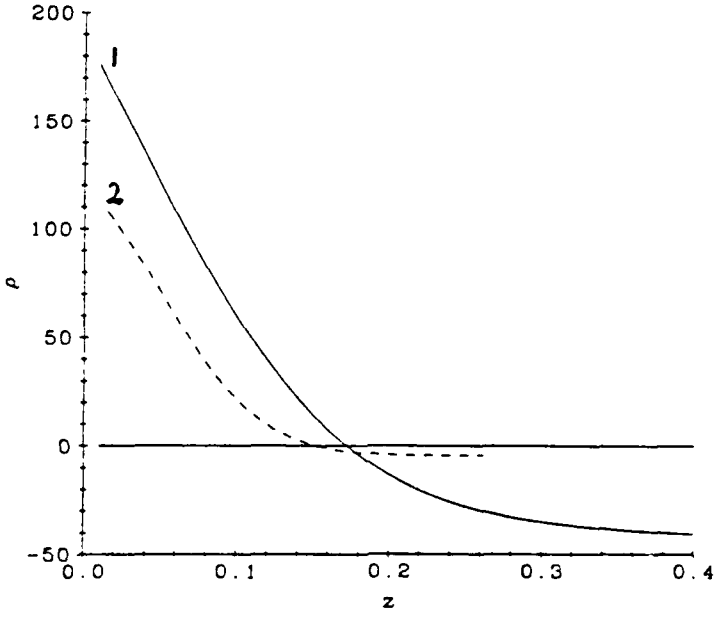

Figure 8. Comparison of Net Space Charge Densities, ρ, for n_s = 0.1, $\mathscr{E}$ = 4 μJ/cm^2, I′ = 50 μW/cm^2 (1) and I′ = 500 mW/cm^2 (2). Taken from Figures 3b and 4, 88 Paper (6:375)

significantly different, even though all experimental data and explanations given up until now indicate that they should be similar, or at least produce similar transverse fields, indicating reciprocity. The unexpected differences in the two space charge distributions prompted us to develop a simple criterion by which to gauge the transverse fields, and subsequent response, produced by a given one-dimensional space charge distribution. This criterion is detailed in the next paragraph. An even more puzzling aspect highlighted by Figure 8 is the fact that the high intensity illumination produces a smaller and narrower space charge region than the low intensity illumination. This is opposite from the effect one would expect from previous explanations.

Since the authors never explain the exact connection between net positive charge distribution and response, we must establish some definite criterion for determining whether two one-dimensional space charge plots produce the same response, within a 30 percent tolerance as specified in the 1988 paper (6:374). Remembering that PRIZ response is due to transverse electric fields within the crystal, we need a criterion that consistently represents the response produced by the transverse electric fields that result from placing our one-dimensional space charge distribution adjacent to a region with a uniformly zero space charge distribution. The boundary between our space charge distribution and the adjacent net zero distribution corresponds to the edge of the slit that is imaged onto the device by the write light. Since the authors assert that the response is due to both the magnitude of the density of positive charge and the thickness of the positive

charge layer, the criterion we will use is the area under the positive portion of the net space charge curve (6:375). If the areas under two different curves are within 30 percent of each other, we will assume that they produce responses within 30 percent of each other. Using this criterion alone, the curves in Figure 8 do not represent reciprocity. The crudeness of our criterion does not allow a total rejection of reciprocity in this case, or in many other cases which we will analyze. Our results in the next section are just as much a test of the validity of our criterion as they are a study of reciprocity. Nevertheless, we felt some value could be obtained from even a crude attempt to characterize the response produced by a given one-dimensional space charge distribution. Perhaps the most obvious weakness of our criterion is the total disregard of the transverse fields produced by the region of net negative space charge density. Other weaknesses will be discussed in the next section.

In concluding the paper, the authors assert that the response of the PRIZ lags the illumination of the writing light for conditions of high intensity illumination and corresponding low exposure times. This will occur any time the exposure time is of the same magnitude or less than the drift time of an electron that has been photogenerated. This final comment sheds a little more light on the authors' claims concerning reciprocity. Accepting Figure 8 as the true depiction of the space charge distributions for high and low intensity illumination, in spite of previously mentioned discrepancies, the effects of lag time can be used to account for the apparent lack of reciprocity. Lag time

explains that the space charge distribution for the high intensity illumination is not as great since charge separation has only begun. Perhaps, if the response is measured after the PRIZ has had time to develop, the high intensity space charge curve should shift outward and indicate reciprocity. The shift, or decay, of space charge distributions following turn-off of the write light will be investigated in the next section. The authors appear to indicate that the effects of lag time and lack of injection at high intensity exposures counteract each other and produce a combined effect that demonstrates reciprocity, relative to the corresponding low intensity situation.

The 1987 paper ultimately investigates two-dimensional aspects of dynamic image selection (DIS), an operating mode of the PRIZ in which stationary inputs are suppressed while moving inputs are imaged. As they state in the preamble, "It is shown that the dominant role in the onset of the response of the modulator to the turn-off of the writing light is played by a mechanism involving the spatially nonuniform injection of electrons into the volume of the crystal through the negative electrode-crystal contact." (5:750) In arriving at this conclusion, the authors present experimental data on the time evolution of diffraction efficiency for writing light intensities of 30 $\mu W/cm^2$ and for various values of the turn-off time, or exposure. One of the primary features of this data is the increasing of diffraction efficiency with exposure for low exposures. This is consistent with data in the 1988 paper if one accepts diffraction efficiency and response as similar parameters. The authors then assert that for higher

exposures, the curves immediately plunge to zero following turn-off of the write beam and then proceed to regenerate themselves. Depending upon interpretation, this data modifies or perhaps even contradicts data in the 1988 paper. Unfortunately, limitations of our one-dimensional models did not permit adequate examination of these apparent contradictions or the phenomena of regeneration.

Specific Modelling Goals

Our modelling goals are divided into four major categories, which will be presented separately in section V. These categories are reproduction of low intensity data (Figures 5 and 6), reproduction of high intensity data (Figure 7), demonstrations of reciprocity (Figures 3 and 8), and demonstrations of self erasure (Figure 3).

Prior to the first category, reproduction of low intensity data, we will include a validation of our two master models. We will accomplish this using the intensity and exposure data specified for Figures 5 and 6. In addition to the data presented in these figures, however, we will also present data for the DI PRIZ, and qualitatively analyze the DI data's consistency relative to the SI and conducting PRIZ data. After validating the master models, we will attempt to reproduce Figures 5 and 6.

In the second category, reproduction of high intensity data, we will attempt to reproduce Figure 7. We will also verify that the corresponding plots for an SI PRIZ differ by less than one percent as the authors assert. Attempts will also be made to verify the statement that, "as the intensity of the writing light increases, the range of

exposures at which injection has only insignificant effect becomes broader." (6:375)

In the third category, demonstrations of reciprocity, we will present a full range of data, similar to that contained in Figure 8, to validate the experimentally established reciprocity region. This will include runs at a wide range of intensities and exposures for both the SI and conducting PRIZ. This should shed light on the assertion that the response of the PRIZ is due to the net positive space charge density near the cathode.

The fourth category will investigate the phenomena of self erasure. Self erasure is demonstrated in Figure 3 by the fact that response eventually appears to decrease, with increased exposure, for all intensities. Once again, since PRIZ response is a multi-dimensional phenomenon, we must intuitively speculate on the nature of the transverse fields produced when our one-dimensional space charge distribution is placed adjacent to a net zero space charge distribution. Using this analogy, we should be able to shed some light on the Russians' assertions concerning the correspondence of PRIZ response to the net positive space charge density near the cathode.

V. Results

Model Validation

Before applying our two master models, we validated them by analyzing the data they produced for an SI, conducting, and DI PRIZ under conditions corresponding to Figures 5 and 6 ($I' = 50\ \mu W/cm^2$, $\mathcal{E}' = 4\ \mu J/cm^2$, $n_s = 0$ for SI and DI, $n_s = 0.1$ for conducting). Three validation runs were made for each of the PRIZ types. These runs corresponded to master model one with parameter set one, master model two with parameter set one, and master model two with parameter set two. The two parameter sets are listed in Table 2 with appropriate references to justify respective values. The primary differences between the two parameter sets are values for electron mobility, density of donors, and absorption coefficient. Parameter set one contains values that appear to predominate in most of the Russian references. Many of the values in parameter set two are taken from references by Peltier, Micheron, Horwitz, and Corbett (30:3683, 25:353). Two parameters that require additional explanation are the donor recombination coefficient and the trap recombination coefficient. The value for the trap recombination coefficient, ζ_t, is obtained from experimental data for times such that $n_- << N_t$. Thus, its value is estimated by multiplying the average electron drift time, τ_d, by the density of traps, N_t. In effect, this transformation modifies the average electron drift time to account for the depletion of traps term in master model one. The slight discrepancy in the value for ζ_t reported in Table 2, 362 reported versus 329 actual,

Table 2

Parameter Sets

Parameter	Parameter Set 1 Value (Reference)	Parameter Set 2 Value (Reference)	Additional References
nbin	100	100	
η	1 (14:1491)	1 (38:1677)	
ν' (Hz)	$6.8 \cdot 10^{14}$	$6.8 \cdot 10^{14}$	(6:374)
V_0' (V)	2000	2000	(6:374)
d_0' (cm)	0.045	0.045	(6:374)
μ ($cm^2/V \cdot sec$)	0.01 (14:1487)	0.03 (25:360)	(8:1532)
t_0' (sec)	$1.0125 \cdot 10^{-4}$	$3.375 \cdot 10^{-5}$	
ϵ_r	50 (8:1532)	56 (25:360)	(14:1491)
ϵ (F/m)	$4.427 \cdot 10^{-10}$	$4.958 \cdot 10^{-10}$	
e (C)	$1.6022 \cdot 10^{-19}$	$1.6022 \cdot 10^{-19}$	
n_0' (cm^{-3})	$2.729 \cdot 10^{13}$	$3.056 \cdot 10^{13}$	
α' (cm^{-1})	40 (38:1673)	45 (11:1689)	
α	1.8	2.025	
N_d	$1 \cdot 10^5$ (8:1532)	$3.27 \cdot 10^5$ (30:3684)	
N_t	366	-	(30:3684)
τ_d	0.9	0.9	(11:1689)
τ_t	$1 \cdot 10^5$	-	(3:1585)
ζ_d	$3.62 \cdot 10^5$	-	
ζ_t	$3.62 \cdot 10^2$	-	
n_s	0.1	0.09	(6:375)
g (I'=30 $\mu W/cm^2$)	0.006	0.0018	
g (I'=50 $\mu W/cm^2$)	0.01	0.003	
g (I'=300 mW/cm^2)	60	18	
g (I'=500 mW/cm^2)	100	30	

is an artifact of earlier AFIT work on the PRIZ and is not significant. The parameter, ζ_d, is assigned a value several orders of magnitude greater than ζ_t to reflect the much lower probability of a donor recombination event versus a trap recombination, or ionization, event. As mentioned earlier, some parameters will be modified individually in some investigations.

Selected results from the first set of validation runs are contained in the Appendix, Figures 41 to 45. These figures reflect normalized data for the SI, conducting, and DI PRIZ for master model one and parameter set one. Data is plotted in a three-dimensional landscape format versus distance and time, and includes density of ionized donors, density of ionized traps, and density of free electrons. Trends in these plots, as well as other validation data, indicate that master model one qualitatively duplicates the major features of the PRIZ, as described in this report and others. For example, all three types of PRIZ show identical results for density of ionized donors, as reflected in Figure 41. This is expected since, neglecting the relatively insignificant donor recombination term, the rate equation that models this factor is unaffected by the insulating characteristics of the cathode and anode. Data for the density of ionized traps and density of free electrons clearly shows the areas of electron concentration and enhanced trapping as the bottleneck region retreats toward the cathode. The data also shows the accelerated movement of the bottleneck towards the cathode for the conducting versus the SI PRIZ, as can be seen by comparisons of Figures 42 and 43 and Figures 44 and 45. This is primarily due to injection. Validation data for the DI PRIZ showed the area of intense trapping as the electrons bunch at the insulated anode. When the DI plots were rescaled to overcome the dominance of anode electron concentration and trapping, the DI PRIZ data for density of ionized traps and density of free electrons was indistinguishable from the corresponding SI PRIZ data. Data for net charge density clearly

showed the formation of the net positive space charge region near the cathode. The net positive space charge region for the conducting PRIZ was obviously smaller in magnitude and thickness than the corresponding values for the DI and SI PRIZ. As discussed earlier, this reduction is due to injection, and is especially pronounced at low intensity exposures. Electric field data and total current data were, in general, also consistent with expected results.

In addition to the aspects mentioned above, some other data is presented here to further validate master model one. Figure 9, below, shows data on the net charge density that accumulates in the crystal over time. As expected, the DI PRIZ accumulates no net charge, while the SI PRIZ accumulates a net positive charge, since some electrons escape through the anode. The conducting PRIZ accumulates a net negative charge since, in this particular case, more electrons are injected through the cathode than escape through the anode. Figure 10 shows the cathode electric field versus time for the three types of PRIZ. The SI and DI curves show that the cathode field becomes more negative as the positive space charge accumulates near the cathode. The conducting PRIZ cathode field also initially becomes more negative, however, the change is so small as to be imperceptible on the given scale. The behavior of the cathode electric field for the conducting PRIZ, at low intensity exposure, was surprising since we expected the field to become much more negative, a condition that would encourage injection. Figure 11 shows the photocurrent through the three types of PRIZ. As expected, the conducting PRIZ photocurrent is greater due to

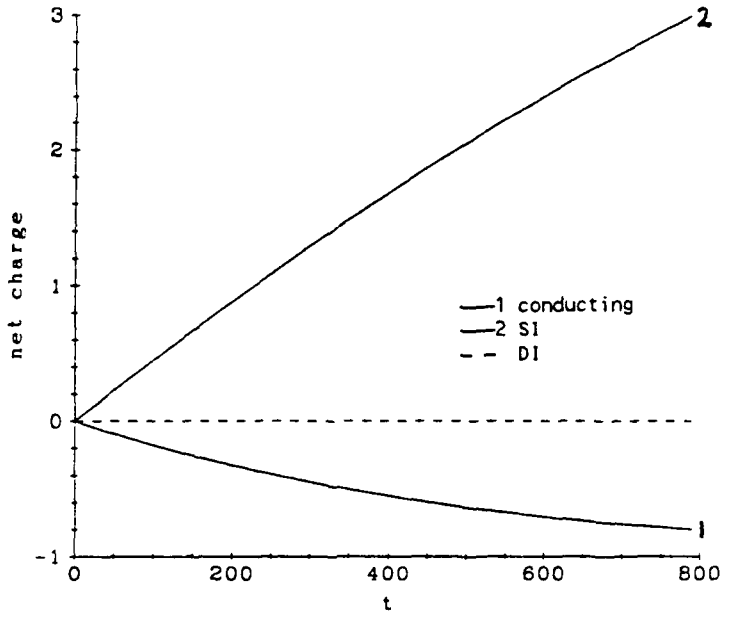

Figure 9. Net Charge Accumulated vs. Time, $I' = 50\ \mu W/cm^2$, $n_s = 0, 0.1$, Master Model One, Parameter Set One

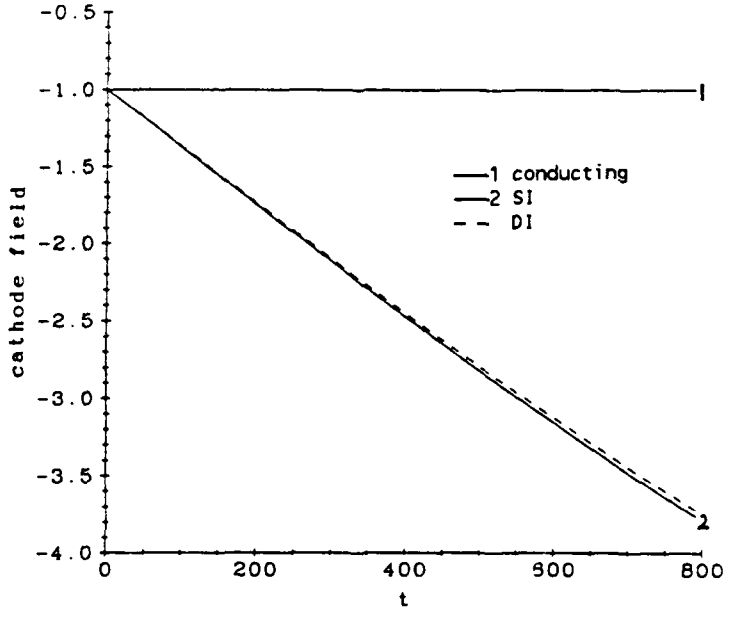

Figure 10. Cathode Electric Field vs. Time, $I' = 50\ \mu W/cm^2$, $n_s = 0, 0.1$, Master Model One, Parameter Set One

injection. The quick rise in photocurrent shows that injection becomes a factor very early in the exposure, as expected for low intensity illumination. Figures 12 and 13 show the net charge density versus time in bins one and two, respectively. As expected, the net charge density in the conducting PRIZ is reduced, versus the SI and DI PRIZ, due to injection. The only surprise encountered in the validation was the extremely small change in the cathode electric field, versus time, for the conducting PRIZ. All the other data, however, indicates that the model is successfully accounting for the effects of injection. After the validation of master model one, computer runs were made for master model two, parameter set one. These runs showed the same qualitative behavior as reported for master model one.

Reproduction of Low Intensity Exposure Data

Next, we attempted to reproduce the Russian data reported in Figures 5 and 6. Figure 14 shows the results of our attempts to reproduce Figure 5, the Russian SI PRIZ data at low intensity exposure ($I' = 50\ \mu W/cm^2$), using both master models and both parameter sets. Although all three combinations of models and parameter sets produced virtually the same results, our data shows charge distributions that are approximately 30 times less than those reported by the Russians. Encouragingly, all exposure curves were qualitatively identical to the Russians' and show the same crossing values for the z axis. Also, the relative magnitudes of all three exposure curves are identical to the relative magnitudes of the Russian curves.

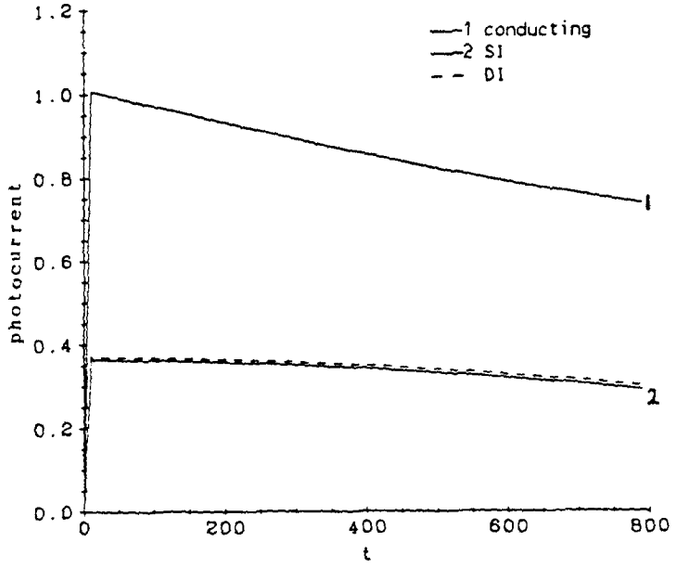

Figure 11. Photocurrent vs. Time, $I' = 50\ \mu W/cm^2$, $n_s = 0, 0.1$, Master Model One, Parameter Set One

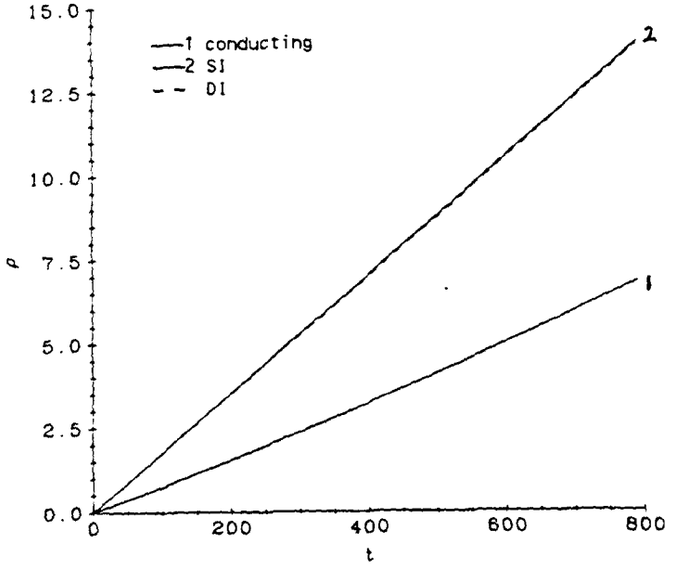

Figure 12. Net Charge Density vs. Time, Bin 1, $I' = 50\ \mu W/cm^2$, $n_s = 0, 0.1$, Master Model One, Parameter Set One

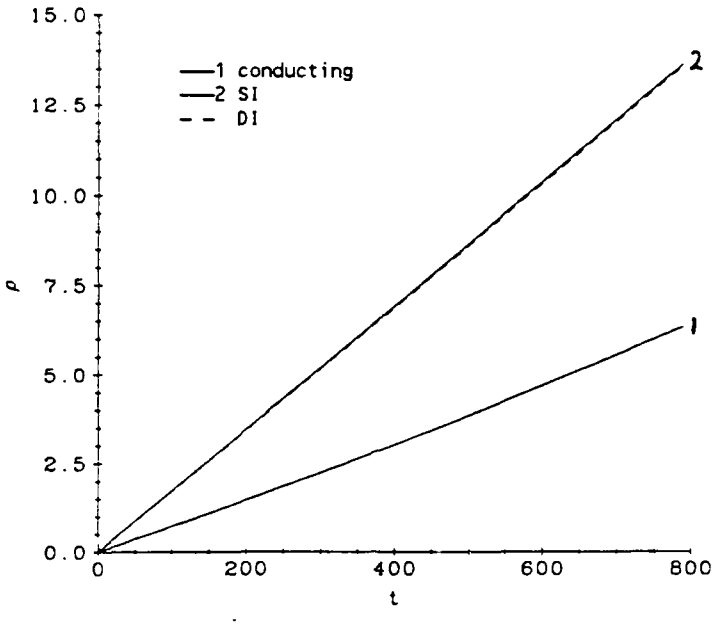

Figure 13. Net Charge Density vs. Time, Bin 2, $I' = 50\ \mu W/cm^2$, $n_s = 0, 0.1$, Master Model One, Parameter Set One

Figure 15 shows the results of our attempts to reproduce Figure 6, the Russian conducting PRIZ data at low intensity exposures. Again, the qualitative aspects of the plots are identical to the Russians' plots, and all three combinations of master models and parameter sets produce similar data. Crossing values are the same as Russian values as are relative magnitudes of the three exposure curves. Most importantly, comparison of Figures 14 and 15 shows that the effects of injection on the charge distribution are identical to effects observed in the Russian plots. Specifically, we can see that both the magnitude and thickness of the positive space charge distributions are reduced by approximately 50 percent due to injection. Despite these successes, however, our plots are once again off by a factor of 30. To improve our quantitative

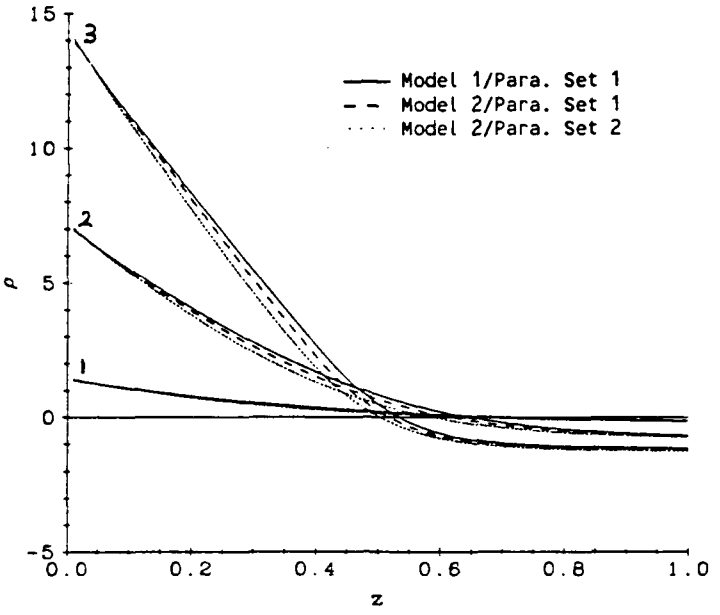

Figure 14. Net Charge Density Distribution. I′ = 50 $\mu W/cm^2$, n_s = 0, $\mathscr{E}$ = 0.4 (1), 2 (2), and 4 $\mu J/cm^2$ (3)

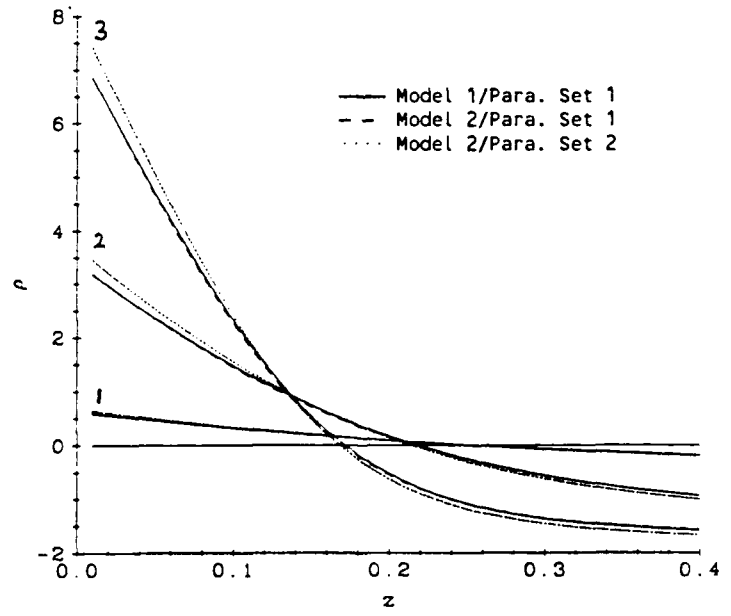

Figure 15. Net Charge Density Distribution, I′ = 50 $\mu W/cm^2$, n_s = 0.1, $\mathscr{E}$ = 0.4 (1), 2 (2), and 4 $\mu J/cm^2$ (3)

agreement with the Russian data, some of the more questionable parameter values were varied to determine their potential effects on quantitative results. Using master model two, parameter set one, and the 4 $\mu J/cm^2$ exposure curve in Figure 14 as a basis, Figure 16 shows the effects of individually varying values for absorption coefficient and average electron drift time. Figure 16 confirms Bryksin's assertion in a 1986 publication that, "the magnitude of the light absorption coefficient is decisive as regards the occurrence of a particular distribution." (9:80) To improve our results by a factor of 30, however, the absorption coefficient must be increased well beyond the value shown in Figure 16 (α = 9, α' = 200 cm^{-1}). This extreme value is not justified for write light wavelengths of 441 nm.

Figure 16 also shows that changing the value of average electron drift time adversely affects crossing values without greatly improving quantitative results. Other factors investigated were density of traps, density of donors, and number of bins. None of these, however, could account for the discrepancies; and combinations of changes in some values, within reasonable bounds, were also unsuccessful. In spite of quantitative discrepancies, modelling of all important qualitative aspects of the Russian data was successful enough to encourage further studies. Figures 17 and 18 highlight the qualitative successes of our low exposure intensity modelling efforts by plotting the Russian data and our data on the same graphs. Our data has been scaled by a factor of 26 and uses master model two with parameter set one.

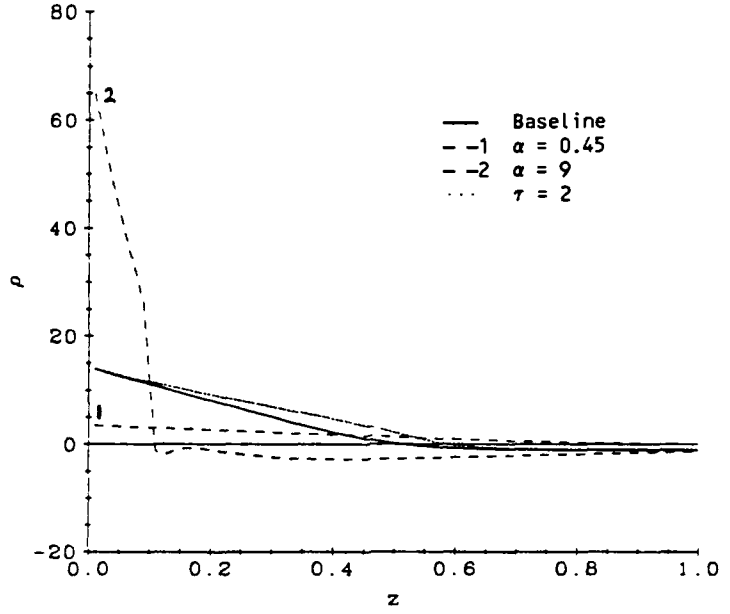

Figure 16. Effects of Absorption Coefficient and Average Electron Drift Time on Net Space Charge Density, $I' = 50\ \mu W/cm^2$, $n_s = 0$, $\mathscr{E} = 4\ \mu J/cm^2$

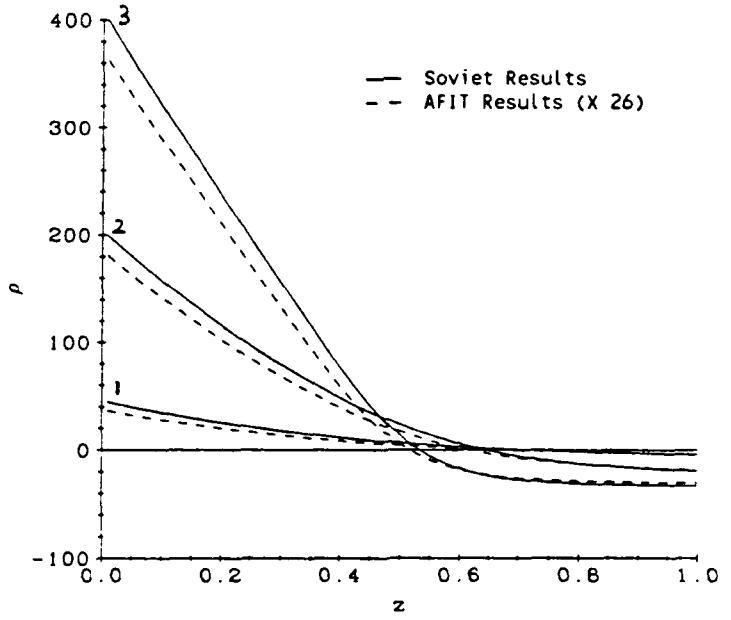

Figure 17. Comparison of Russian Low Intensity Exposure Data with Our Data Scaled up by a Factor of 26, $I' = 50\ \mu W/cm^2$, $n_s = 0$, $\mathscr{E} = 0.4$ (1), 2 (2), and $4 \mu J/cm^2$ (3) (6:375)

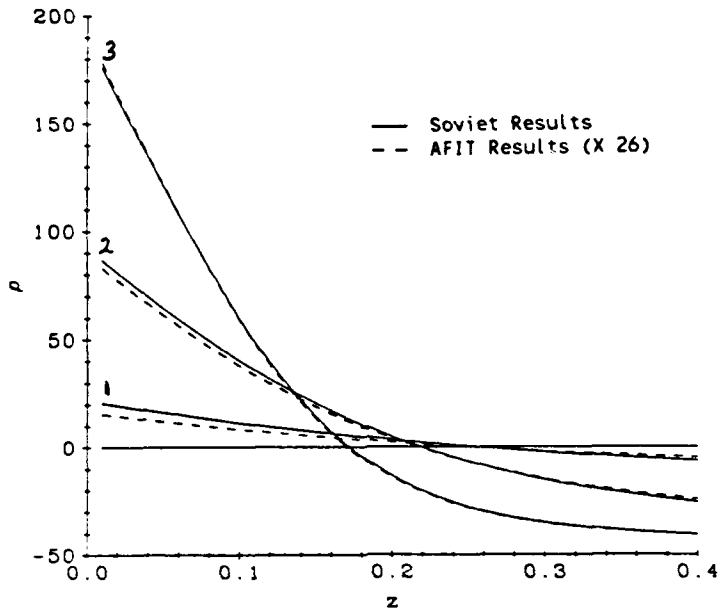

Figure 18. Comparison of Russian Low Intensity Exposure Data with Our Data Scaled up by a Factor of 26, $I' = 50\ \mu W/cm^2$, $n_s = 0.1$, $\mathscr{E} = 0.4$ (1), 2 (2), and $4\mu J/cm^2$ (3) (6:375)

Reproduction of High Intensity Exposure Data

Next, we attempted to reproduce Russian high intensity exposure data ($I' = 500\ mW/cm^2$) shown in Figure 7. Landscape plots showed the same qualitative features used to validate our models at low intensity exposure. Data for net charge density accumulated in the crystal versus time, however, showed one major difference from the low intensity exposure data. The net charge accumulated for a conducting PRIZ was positive, for this particular high intensity exposure, indicating more electrons were extracted from the anode than injected through the cathode. This is consistent with earlier assertions that injection at

high intensities and low exposures is relatively insignificant. Figure 19 shows net charge accumulation for the SI, conducting, and DI PRIZ under high intensity illumination. Figure 20 shows the cathode electric field versus time for high intensity exposures. Once again, the conducting PRIZ data shows striking differences from the corresponding low intensity exposure data. For high intensity, the cathode field for the conducting PRIZ becomes more negative at approximately the same rate as that for the SI and DI PRIZ. This indicates that injection has not yet become significant enough to modify evolution of the space charge, as happens almost immediately for low intensity exposures. Figure 21 shows that the photocurrent through the PRIZ at high intensity exposure is identical for the SI and conducting PRIZ. Likewise, Figures 22 and 23 show that the net charge density versus time in bins one and two are almost identical. All of these features indicate that injection is relatively insignificant at high intensity exposure.

Figure 24 shows our attempts to reproduce Russian data reflected in Figure 7. Once again, the qualitative features of the plot are similar to the Russian data. In this case, however, our magnitudes are only approximately seven times less than the Russians'. Another significant difference is the fact that parameter set two produces significantly different data than parameter set one. The z axis crossings for parameter set two are closer to the Russian values than crossings for parameter set one, although neither set produces crossings as close to the Russian values as we experienced in reproducing low intensity

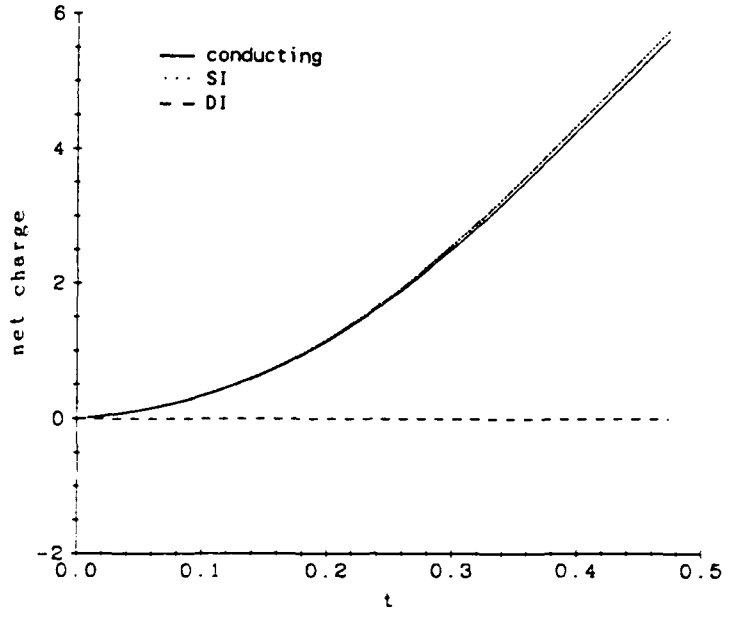

Figure 19. Net Charge Accumulated vs. Time, $I' = 500$ mW/cm^2, $n_s = 0$, 0.1, Master Model One, Parameter Set One

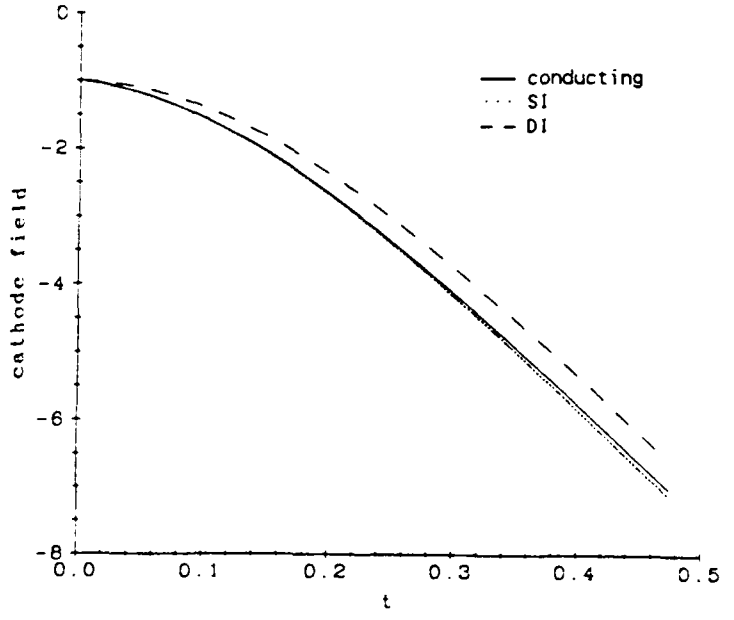

Figure 20. Cathode Electric Field vs. Time, $I' = 500$ mW/cm^2, $n_s = 0$, 0.1, Master Model One, Parameter Set One

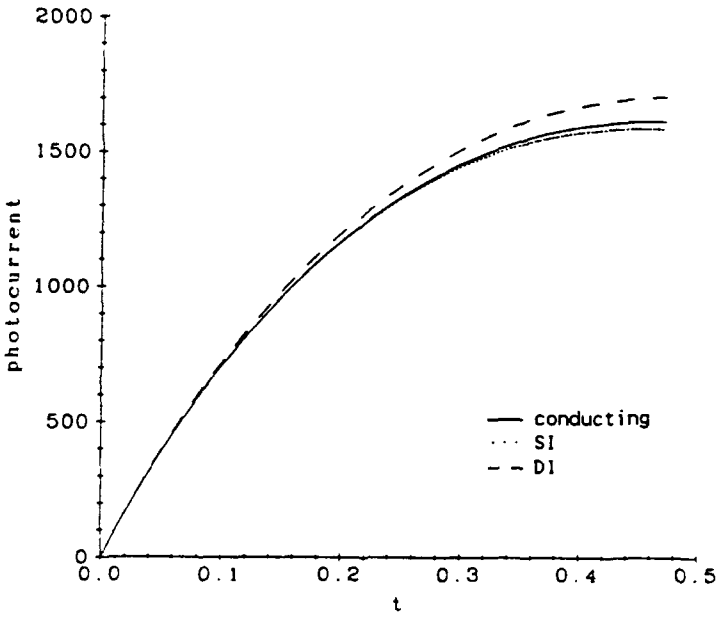

Figure 21. Photocurrent vs. Time, $I' = 500$ mW/cm^2, $n_s = 0, 0.1$, Master Model One, Parameter Set One

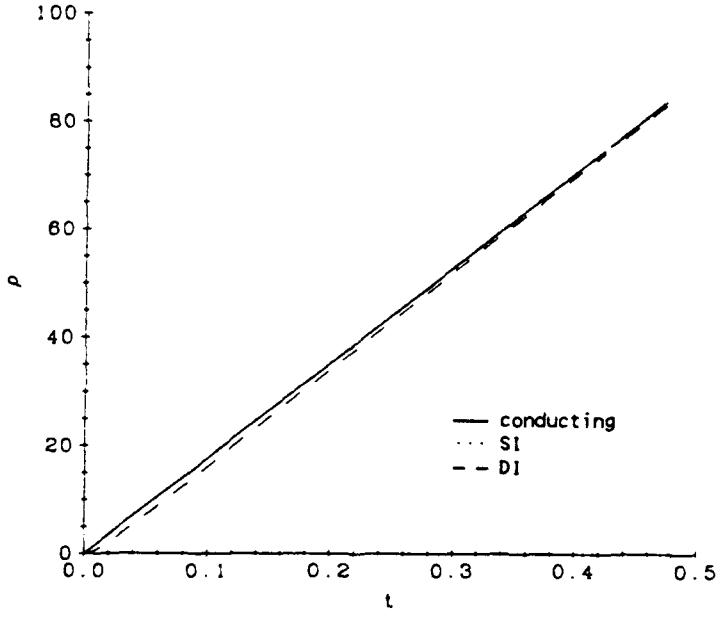

Figure 22. Net Charge Density vs. Time, Bin 1, $I' = 500$ mW/cm^2, $n_s = 0, 0.1$, Master Model One, Parameter Set One

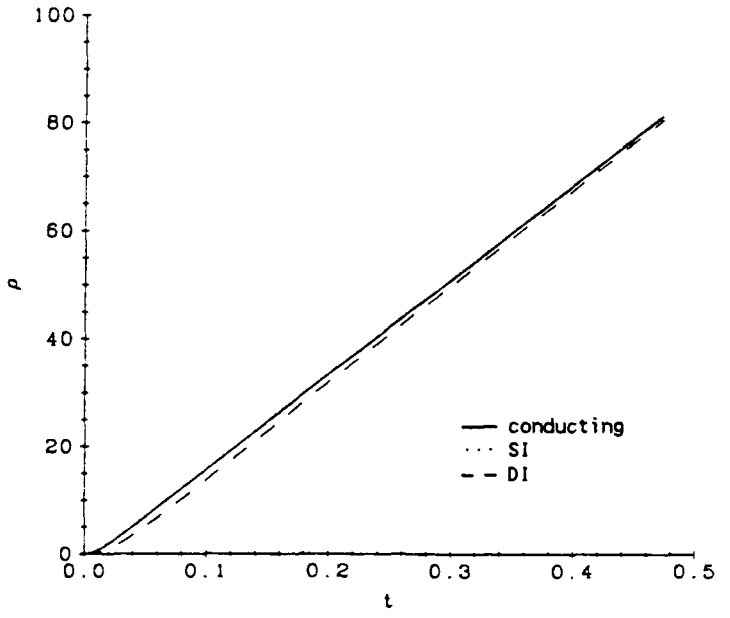

Figure 23. Net Charge Density vs. Time, Bin 2, I′ = 500 mW/cm^2, n_s = 0, 0.1, Master Model One, Parameter Set One

exposure data. The shift of crossings to higher z values for parameter set two is primarily due to the increased electron mobility (μ = 0.03 cm^2/V•sec for set two, μ =0.01 cm^2/V•sec for set one), which allows the photogenerated electrons to drift more rapidly, enhancing net positive charge development. Figure 25 shows plots of the Russians' and our high intensity exposure data on the same graph. Our data has been scaled upward by a factor of seven and reflects data for a conducting PRIZ using master model two and parameter set one. Again, the reasons for the discrepancies in quantitative results are unclear. The fact that the discrepancy is seven for high intensity plots and 30 for low intensity plots is inexplicable. As for low intensity exposures,

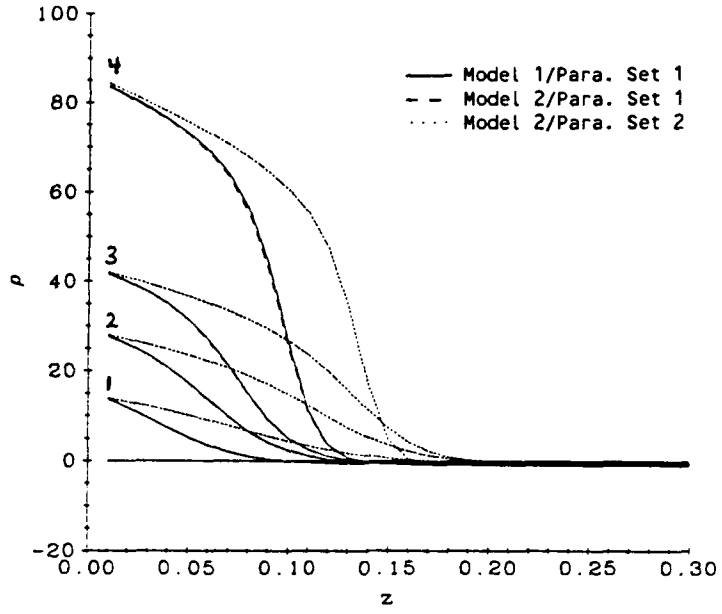

Figure 24. Net Charge Density Distribution, $I' = 500$ mW/cm^2, $n_s = 0.1$, $\mathscr{E} = 4$ (1), 8 (2), 12 (3), 24 μJ/cm^2 (4)

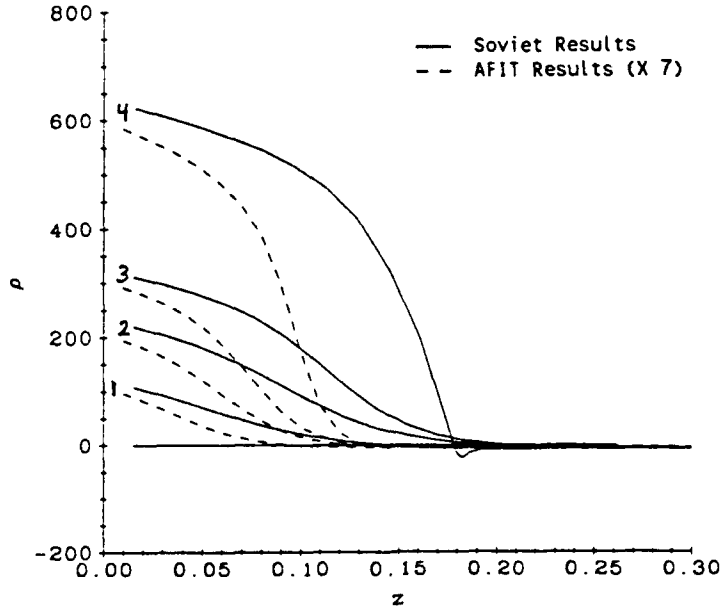

Figure 25. Comparison of Russian High Intensity Exposure Data with Our Data Scaled up by a Factor of 7, $I' = 500$ mW/cm^2, $n_s = 0.1$, $\mathscr{E} = 4$ (1), 8 (2), 12 (3), and 24 μJ/cm^2 (4) (6:375)

attempts were made to modify parameters, within reasonable bounds, to account for the factor of seven discrepancy. Plots with individually varied parameters such as number of bins, absorption coefficient, average electron drift time, density of donors, and density of traps, however, could not account for the discrepancies.

Next, we made attempts to demonstrate the 1988 paper's assertions that data in Figure 7 differs by less than one percent for an SI PRIZ (6:375). Since we could not quantitatively reproduce their data in Figure 7, we had to rely on comparisons for an SI and a conducting PRIZ using data we had generated in Figure 24. Figure 26 demonstrates that the assertion is accurate, using our data from master model two and parameter set one. Though data for a DI PRIZ showed significant deviations, the SI and conducting PRIZ data for all exposures shown is virtually identical. Figure 26 reinforces previous assertions concerning the relative insignificance of injection at high intensities and low exposures.

Finally, we analyzed the 1988 paper's assertion that, "As the intensity of the writing light increases, the range of exposures at which injection has only insignificant effect becomes broader." (6:375) Figures 27 to 29 show plots of net charge density versus z for exposures of 4 and 40 $\mu J/cm^2$ and intensities of 30 $\mu W/cm^2$, 3 mW/cm^2, and 300 mW/cm^2, respectively. These plots show that the assertion given above is also accurate, using data from master model two and parameter set one.

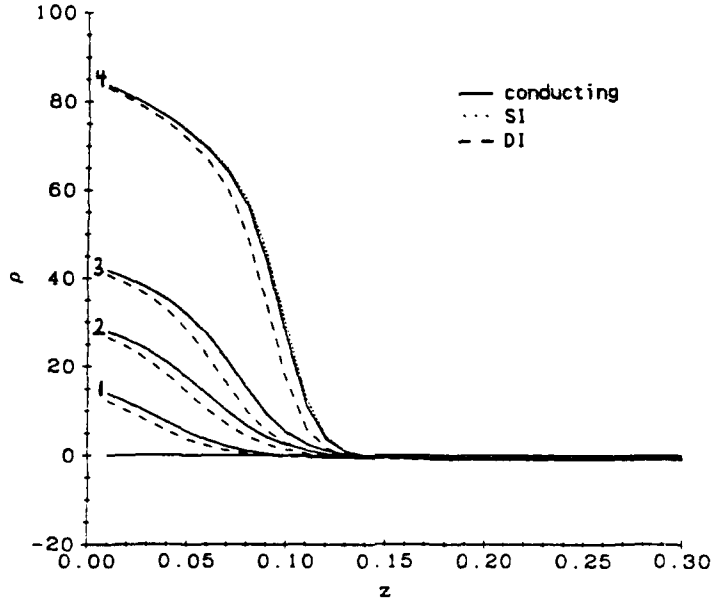

Figure 26. Comparison of High Intensity Exposure Data for an SI and a Conducting PRIZ, $I' = 500$ mW/cm^2, $n_s = 0$, 0.1, $\mathscr{E} = 4$ (1), 8 (2), 12 (3), and 24 μJ/cm^2 (4)

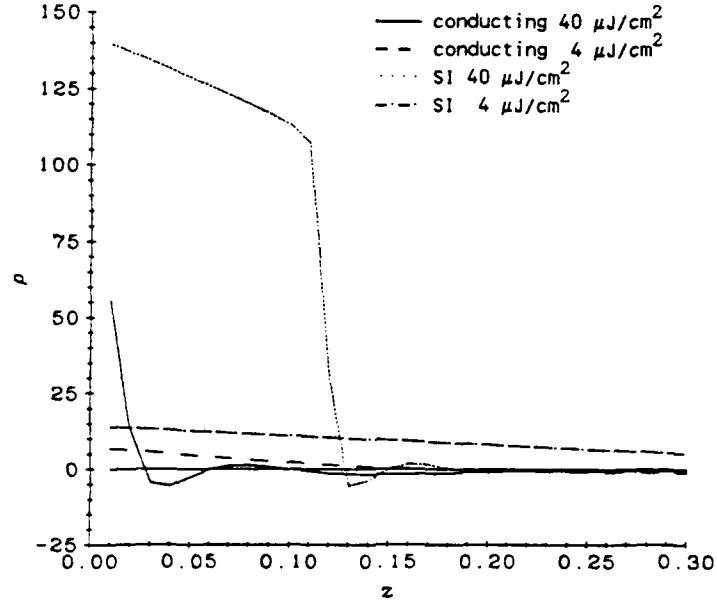

Figure 27. Comparison of Low Intensity Exposure Data for an SI and a Conducting PRIZ, $I' = 30$ μW/cm^2, $n_s = 0$, 0.1, $\mathscr{E} = 4$ and 40 μJ/cm^2

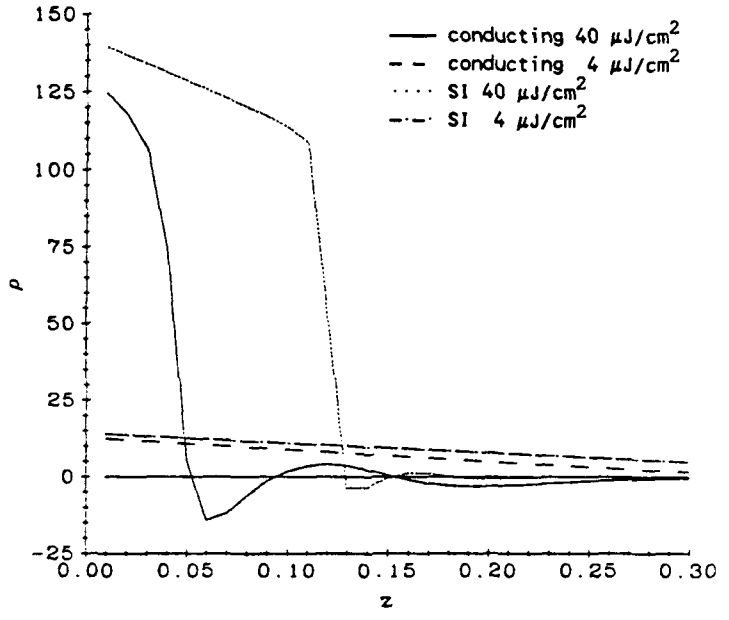

Figure 28. Comparison of Medium Intensity Exposure Data for an SI and a Conducting PRIZ, $I' = 3$ mW/cm^2, $n_s = 0$, 0.1, $\mathscr{E} = 4$ and 40 μJ/cm^2

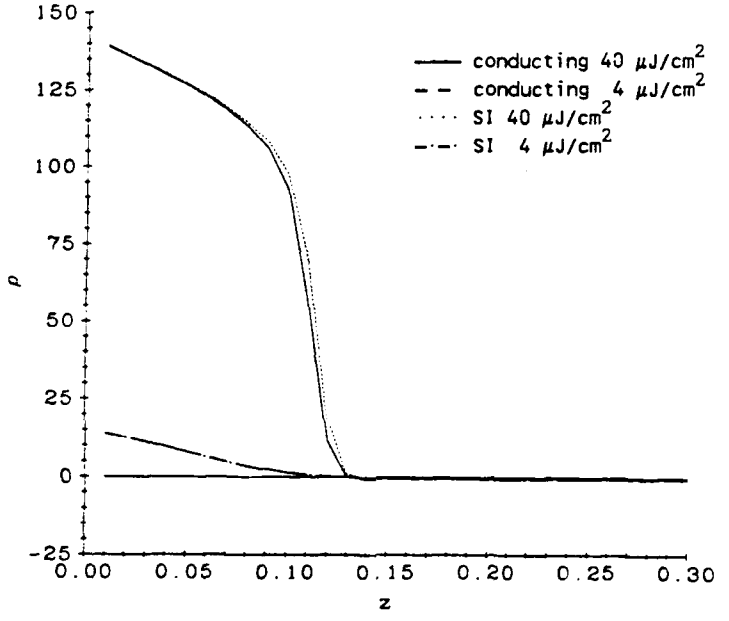

Figure 29. Comparison of High Intensity Exposure Data for an SI and a Conducting PRIZ, $I' = 300$ mW/cm^2, $n_s = 0$, 0.1, $\mathscr{E} = 4$ and 40 μJ/cm^2

Investigations of Reciprocity

Before attempting to reproduce reciprocity data, we analyzed the development of the net charge distribution, of the SI and conducting PRIZ, after turn-off of the write light. Data for the DI PRIZ was virtually identical to that for the SI PRIZ and will not be discussed separately. When the write light is turned off, the evolution of the net charge distribution depends on the injecting characteristics of the cathode, material properties of the PRIZ crystal, such as electron mobility, and lag time effects. Lag time effects are, as previously discussed, more prevalent at high intensities and low exposure times, where the charge distribution has not had time to fully develop. Analysis was accomplished by continuing the calculations of the differential equations after setting the generation coefficient to zero. Results for all low intensity runs ($I' = 30\ \mu W/cm^2$) showed that the net space charge distributions did not change perceptibly after the PRIZ was allowed to decay, or relax, for up to 10 time constants ($10 \cdot t_0' \approx 1$ msec) past write light turn-off. This held true for the SI, conducting, and DI PRIZ and reflects the inherent optical storage capabilities of the PRIZ. Basically, for low intensity illumination, the characteristic exposure times allow the charge separation to continually develop throughout the exposure process. Therefore, when the write light is turned off, little additional charge separation is left to occur. For high intensity illumination, however, the relaxation process was more evident, as illustrated in Figures 30 and 31 for the SI and conducting PRIZ, respectively. The net space charge distribution in the SI PRIZ

widens at a progressively slower rate after turn-off of the write light. Most of the additional net positive space charge distribution, however, occurs during the first time constant past write light turn-off. Our analysis only considered relaxation times up to ten time constants. Eventually, of course, the positive space charge distribution will decay due to thermal ionization, which is represented in master model one, and other equilibrium processes. Relaxation in the conducting PRIZ is significantly different as evident from Figure 31. After turn-off of the write light the net positive space charge region initially expands but quickly contracts again. The maximum net space charge region appears to occur after one time constant.

Referring back to Figure 8, the relaxation characteristics mentioned above could explain why the curves for high and low intensity exposures do not exhibit reciprocity, using our criterion for total area under the net positive space charge curve. If response measurements are made one time constant following the completion of a given exposure, then the low intensity curve will be unaffected while the high intensity curve will expand out to encompass more total area. In doing so, the resulting curves could meet our reciprocity criterion. Unfortunately, however, reproduction of Figure 8 using our data for high and low intensity exposures did not even qualitatively resemble the Russian data, as shown in Figure 32. Our data indicates that the curves exhibit reciprocity without accounting for relaxation. Reciprocity fails, in our data, if a one time constant delay is used prior to measuring

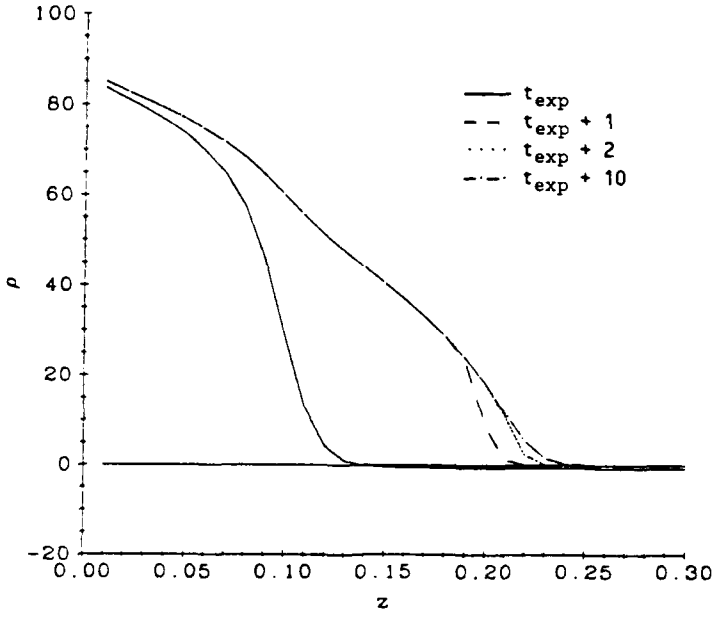

Figure 30. Relaxation of Net Positive Space Charge Following Turn-off of Write Light, $I' = 500\ mW/cm^2$, $n_s = 0$, $\mathscr{E} = 24\ \mu J/cm^2$

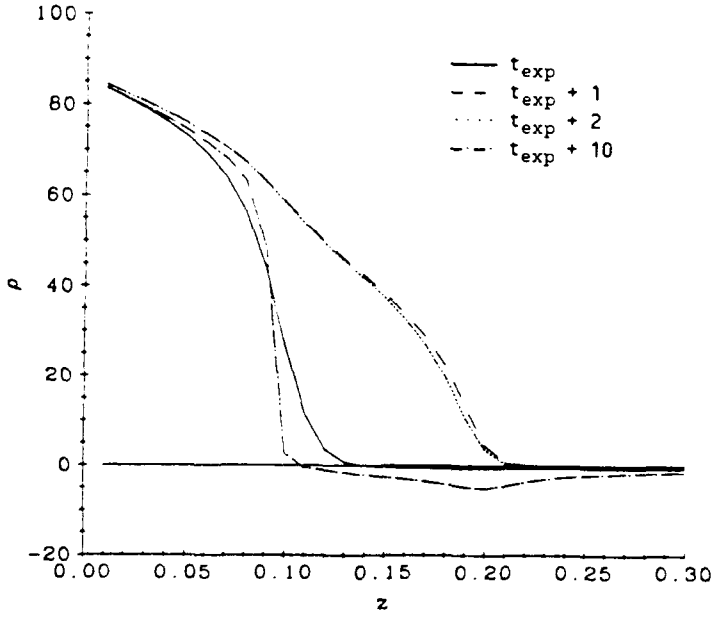

Figure 31. Relaxation of Net Positive Space Charge Following Turn-off of Write Light, $I' = 500\ mW/cm^2$, $n_s = 0.1$, $\mathscr{E} = 24\ \mu J/cm^2$

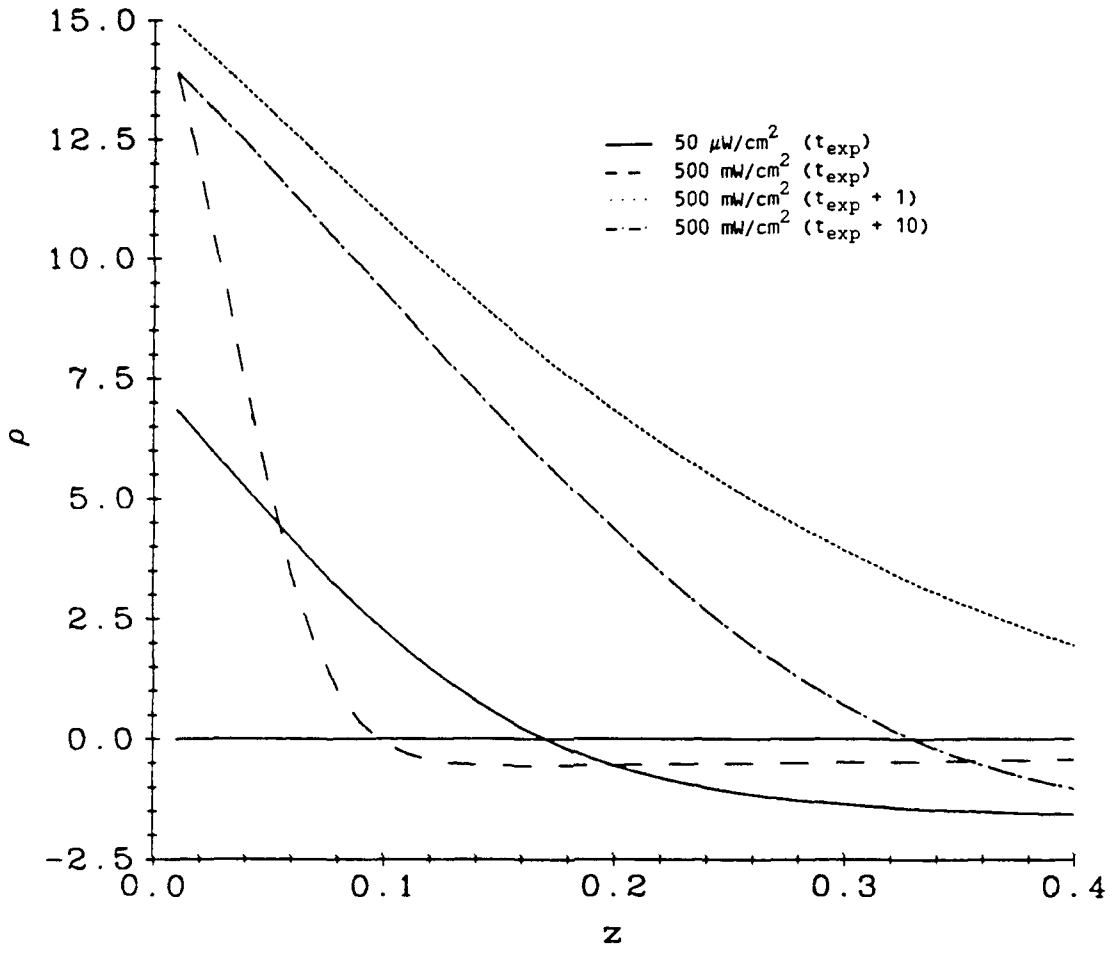

Figure 32. Relaxation Distribution of Net Space Charge for High (500 mW/cm^2) and Low (50 μW/cm^2) Intensity Exposures, n_s = 0.1, $\mathscr{E}$ = 4 μJ/cm^2

response. Further analysis indicates that the apparent reciprocity shown by our data in Figure 32 is not indicative of an overall trend.

To further investigate reciprocity, we analyzed net space charge density data for an SI and a conducting PRIZ at write light intensities from 30 μW/cm^2 to 300 mW/cm^2 and exposures from 4 to 40 μJ/cm^2. The intensities correspond to those in the 1988 paper for which reciprocity was experimentally analyzed, and the exposures correspond to values

within and without the experimentally established region of reciprocity. Net charge density data was recorded for both types of PRIZ, and for several intensities and exposures, at times corresponding to zero delay and one time constant delay. The results for the SI PRIZ, using no delay in recording the net space charge density, are shown in Figure 33. This figure indicates that the SI PRIZ with no delay is not reciprocal at the three lower exposure values (4, 12, and 20 $\mu J/cm^2$), but becomes reciprocal at the higher exposure value of 40 $\mu J/cm^2$. Figure 34, however, indicates that the SI PRIZ exhibits reciprocity at all exposure and intensity values when a one time constant delay is used. Figure 35 shows that the conducting PRIZ, with no time delay, thoroughly fails our reciprocity criterion. Figure 36 indicates that the conducting PRIZ with a one time constant delay fails even more thoroughly.

Reciprocity appears to defy description in one dimension. One possible explanation for our failures in this respect is contained in a 1984 publication by Bryksin. Bryksin states, "We emphasize that the negative space charge region has a greater influence than the positive space charge region on the integrated characteristic for the transverse field because it is located farther away from the negative metal electrode." (12:881) On the other hand, Petrov states in a 1989 paper that "the total positive charge is usually considerably larger than the negative one, and thus we can justifiably neglect the readout light modulation via the negative charge field." (32:337) Although these two statements appear contradictory, the specific contexts in which they are applied remove the ambiguity. Bryksin's statement applies to space

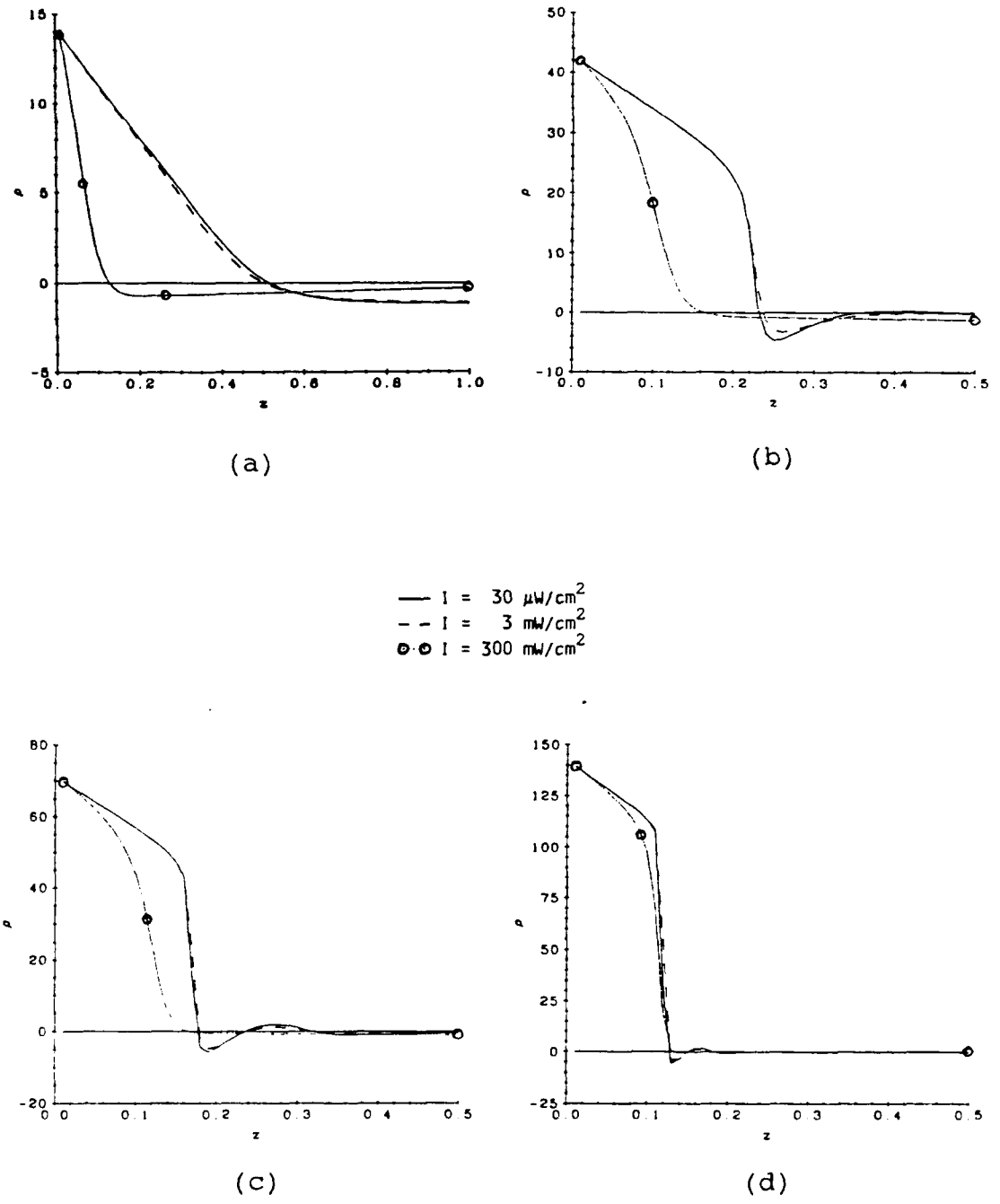

Figure 33. Distribution of Net Space Charge in an SI PRIZ with no Delay in Recording Response, $\mathscr{E}$ = 4 (a), 12 (b), 20 (c), and 40 $\mu J/cm^2$ (d)

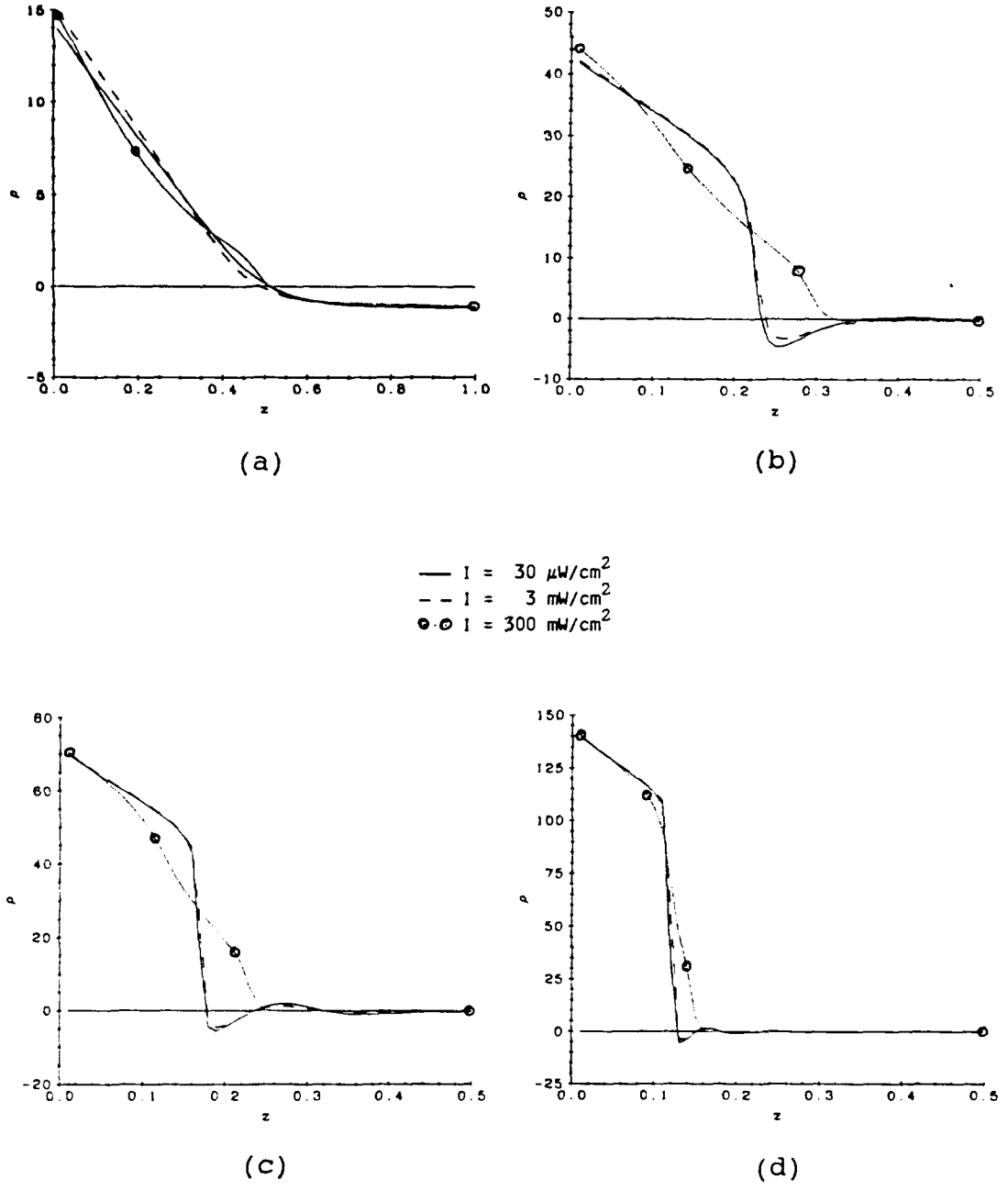

Figure 34. Distribution of Net Space Charge in an SI PRIZ with a One Time Constant Delay in Recording Response, $\mathscr{E}$ = 4 (a), 12 (b), 20 (c), and 40 $\mu J/cm^2$ (d)

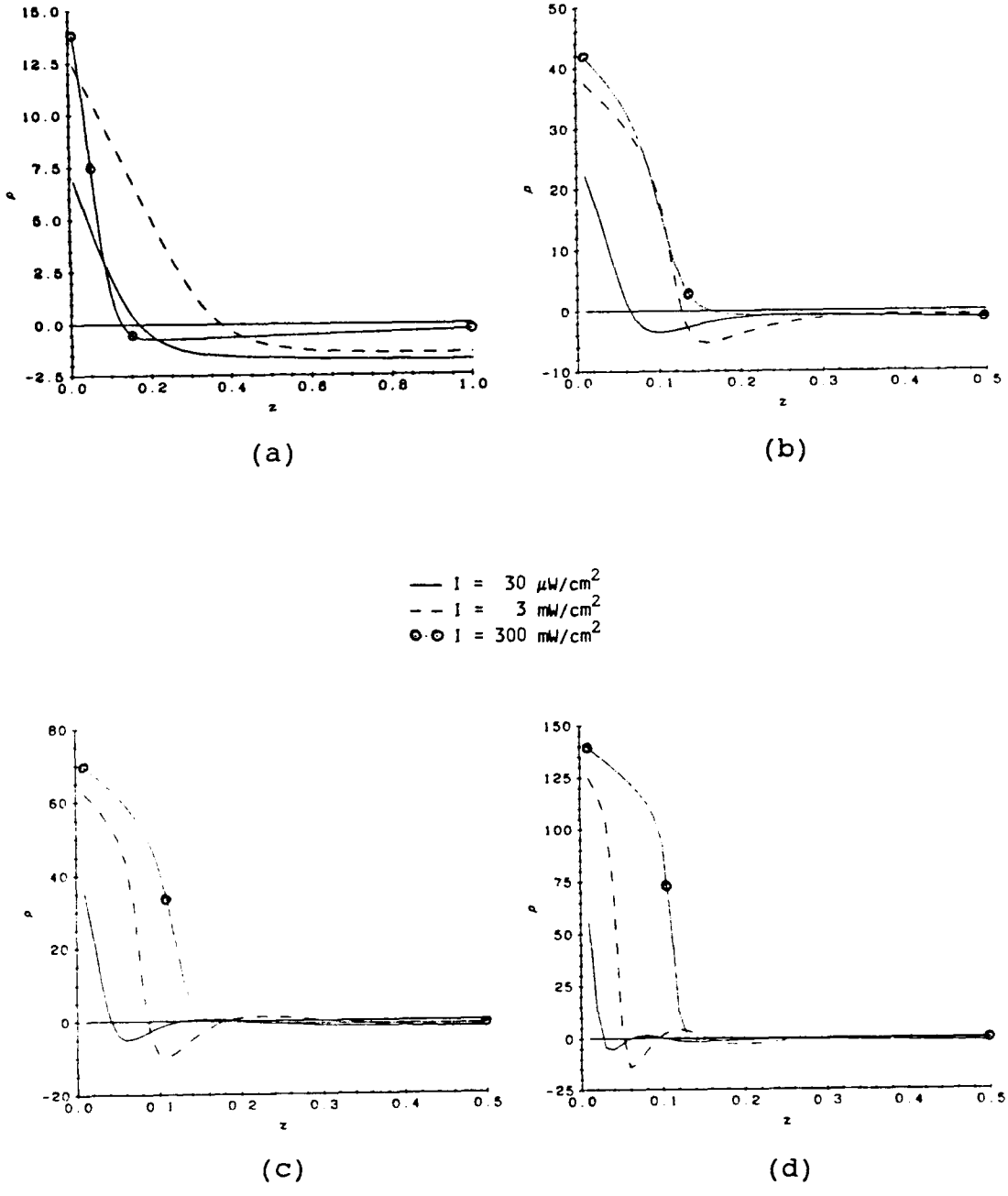

Figure 35. Distribution of Net Space Charge in a Conducting PRIZ with no Delay in Recording Response, $n_s = 0.1$, $\mathscr{E} = 4$ (a), 12 (b), 20 (c), and 40 $\mu J/cm^2$ (d)

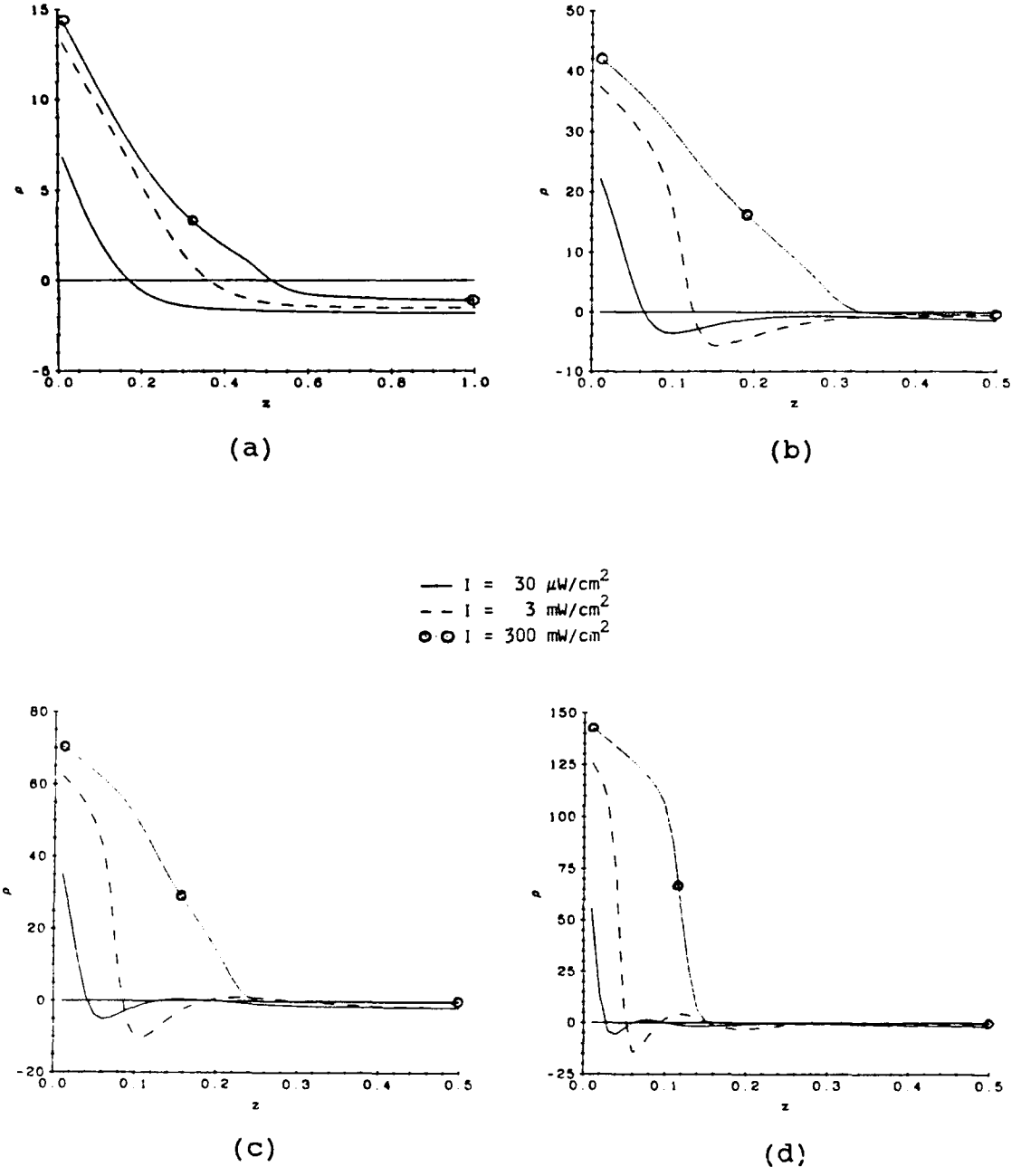

Figure 36. Distribution of Net Space Charge in a Conducting PRIZ with a One Time Constant Delay in Recording Response, $n_s = 0.1$, $\tilde{\mathcal{E}} = 4$ (a), 12 (b), 20 (c), and 40 $\mu J/cm^2$ (d)

charge distributions that have significant regions of both positive and negative space charge. Figure 18 on page 61 shows such a situation for low intensity exposure. Petrov is referring to distributions in which the positive space charge region is dominant. Figure 25 on page 66 shows this situation for high intensity exposure. The specific nature of the space charge distribution determines the approximations we can use to predict the response. Our simple criterion for predicting response, based on the total area of the positive space charge region, is inadequate for distributions with a significant negative space charge region.

Investigations of Self Erasure

The first figures in both the 1987 and 1988 papers indicate a phenomenon called self erasure. Self erasure occurs when the PRIZ response, due to a stationary image, develops peaks and then starts to diminish. In some cases, the image is completely erased despite continuous imaging. Figure 3 depicts the phenomenon of self erasure in a conducting PRIZ. Figure 4 shows total exposure values ($\mathscr{E}_{max}$), for various intensities, at which the response of the PRIZ peaks. Exposures beyond these $\mathscr{E}_{max}$ points demonstrate the onset of self erasure. The exposure times to produce self erasure are much greater than any we have analyzed so far. For example, at 50 $\mu W/cm^2$, the greatest exposure time we have analyzed up until now is 80 msec ($\mathscr{E} \approx 4\ \mu J/cm^2$). To experience self erasure at this intensity, we must use exposure times greater than one second. For 500 mW/cm^2, we have analyzed exposure times of 48 μsec

($\mathcal{E} \approx 24\ \mu J/cm^2$). To experience self erasure at this intensity, we must use exposure times greater than one millisecond.

To analyze self erasure in one dimension, we used intensities of 30 $\mu W/cm^2$ and 300 mW/cm^2 with exposure times of 2.7 sec ($\mathcal{E} \approx 80\ \mu J/cm^2$) and 16.2 msec ($\mathcal{E} \approx 4.9\ mJ/cm^2$), respectively. These exposure values should reach well into the self erasure region according to data in Figure 4. Once again, to model the two-dimensional transverse electric field effects using our one-dimensional models, we intuitively analyzed the fields produced when our one-dimensional net space charge distribution is placed adjacent to a net zero space charge region. As we found in our discussions on reciprocity, the overall response produced by this configuration is very complicated. However, if we can show that our charge distribution approaches zero as the exposure increases, then the transverse fields between the two adjacent regions would also approach zero. The absence of transverse fields would result in zero response, indicating self erasure. Certainly, a uniformly zero charge distribution is not the only way to achieve zero response. A favorable combination of positive and negative space charge regions throughout the length of the crystal could conceivably produce transverse fields that result in zero net response. This situation, however, is much more difficult to analyze with one-dimensional models.

Intuitively, we anticipated that, due to the bottleneck effect, the net positive space charge region would retreat toward the cathode as the exposure increased. Whether the bins nearest the cathode would actually diminish to zero net charge density, however, was unclear. Figure 37

indicates that all bins except the first one do indeed go to zero as the exposure increases. Unfortunately, the net charge density in bin two passes through the zero value and becomes increasingly negative. The response produced by such a distribution is difficult to predict. Figure 37 was produced using master model one, parameter set one, and an intensity of 300 mW/cm^2. Since the 1988 paper never specified material parameters for their experiment, however, we varied several of the values in parameter set one in attempts to drive all bins to zero net charge density. Figure 38 shows the results of increasing the cathode injection coefficient, n_s, from 0.1 to 10. As can be seen, the charge in bin two is significantly reduced, although it still eventually becomes negative. Decreasing the average electron drift time, τ_d, to 0.009 versus 0.9 produced data identical to that for $n_s = 10$. Although we were able to affect the charge density in bin two by adjusting parameter values, we were never able to arrest the linear rise of the charge density in bin one. Interestingly, individual plots of density of ionized trap data from master model one indicated that filling of traps occurred throughout the length of the crystal during the course of the exposure. When we switched to master model two, which does not model the depletion of traps, however, we saw little change in the net charge densities in bins one and two.

Figure 39 shows data for master model one, parameter set one, and an intensity of 30 $\mu W/cm^2$. Here, the net charge density in bin one did not continually increase at a linear rate, although it also never decreased. The charge in bin two never goes to zero and appears to

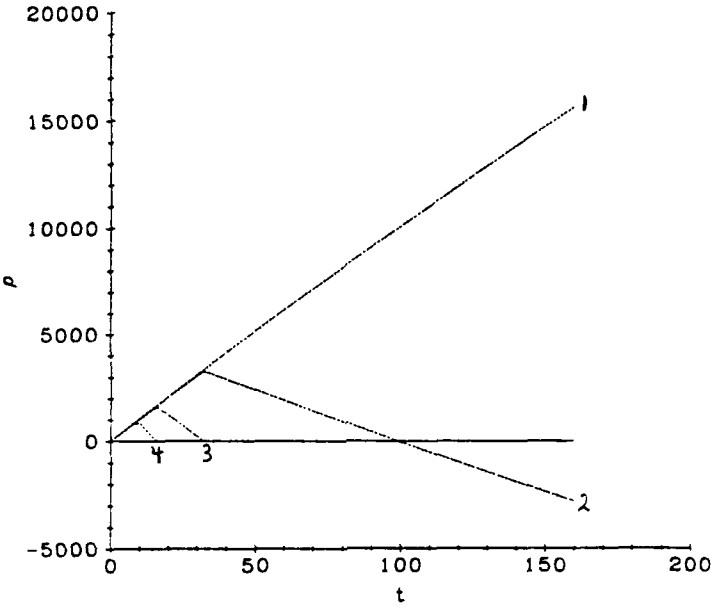

Figure 37. Net Charge Density vs. Time in Bins 1 (1), 2 (2), 3 (3), and 4 (4), $I' = 300\ mW/cm^2$, $n_s = 0.1$, $\mathscr{E} = 0$ to $4.9\ mJ/cm^2$

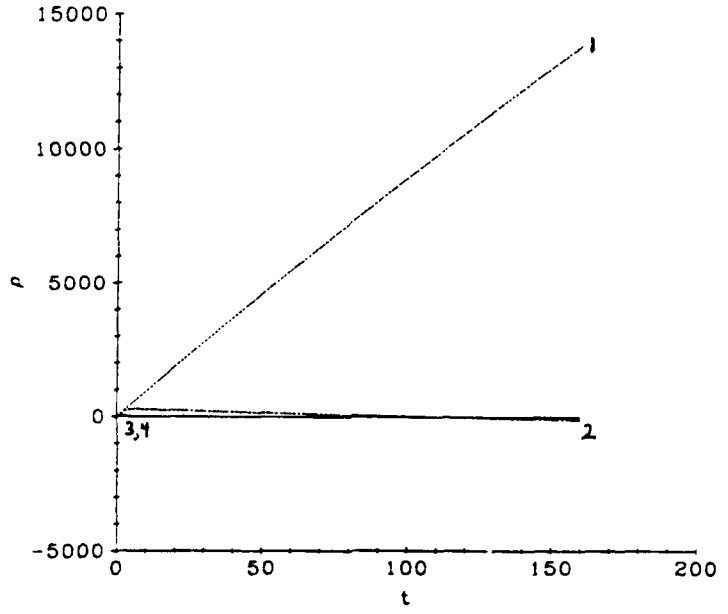

Figure 38. Net Charge Density vs. Time in Bins 1 (1), 2 (2), 3 (3), and 4 (4), $I' = 300\ mW/cm^2$, $n_s = 10$, $\mathscr{E} = 0$ to $4.9\ mJ/cm^2$

level out at a moderately high value of net positive charge density. The charge densities in higher bins approach and sometimes cross zero, then remain at relatively small positive or negative values. Figure 40 shows that by switching to master model two, we were able to force the value of net charge density in all bins, except bin one, towards zero. More significantly, we were also able to cause the net charge density in bin one to level off, although it still never decreased. The differences produced by the two master models indicated that recombination of donors, filling of traps, or detrapping was having a major affect on the results from master model one. None of these effects was observed, however, from individual plots of density of ionized donors or density of ionized traps. More perplexing was the fact that the data showed no sensitivity to changes in n_s from 0.01 to 10. Plots of the cathode electric field versus time revealed that, once again, the cathode field was staying at or near its initial value, a condition that does not allow significant injection. This recurring feature of our analytical data, for low intensity exposures, prompted a more detailed analysis of the specific conditions for which the feature was observed. This analysis showed that when the ratio of the injection coefficient, n_s, to a quantity that characterizes the rate of charge separation, $g\tau_d$, is greater than one, the cathode field exhibited little variation from its initial value. Bryksin previously characterized the behavior of his analytical models with respect to the parameter $n_s/g\tau_d$ in several papers. In his earlier models, he established that values for this parameter must be less than one for accurate results (16:1350).

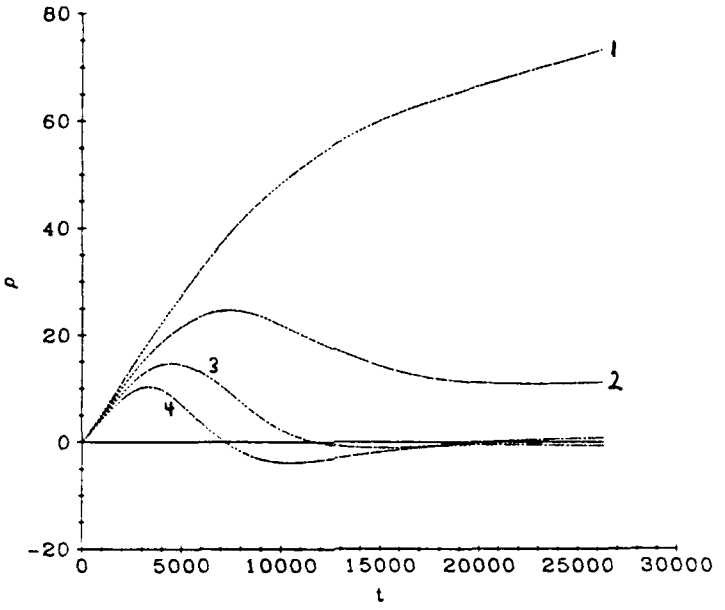

Figure 39. Net Charge Density vs. Time in Bins 1 (1), 2 (2), 3 (3), and 4 (4), $I' = 30\ \mu W/cm^2$, $n_s = 0.1$, $\mathscr{E} = 0$ to 80 $\mu J/cm^2$, Master Model One

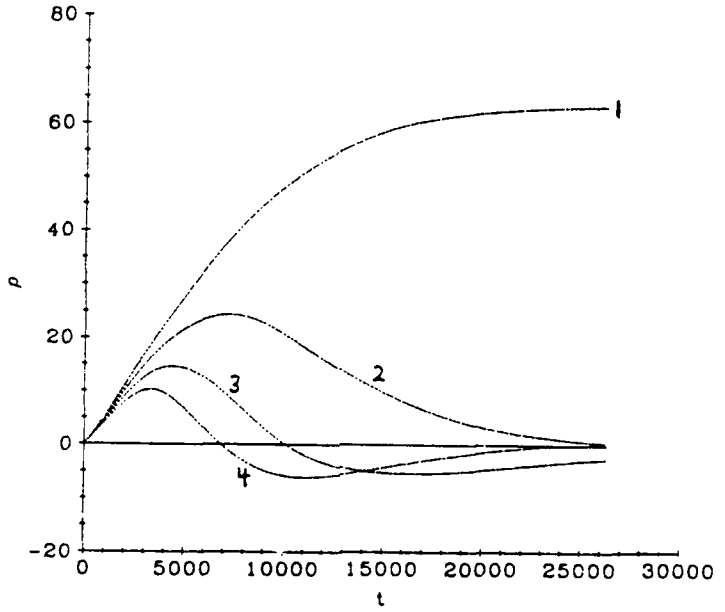

Figure 40. Net Charge Density vs. Time in Bins 1 (1), 2 (2), 3 (3), and 4 (4), $I' = 30\ \mu W/cm^2$, $n_s = 0.1$, $\mathscr{E} = 0$ to 80 $\mu J/cm^2$, Master Model Two

Though subsequent models removed the assumption that mandated this restriction, the behavior of the PRIZ is still tied to the value of this ratio relative to one. For both parameter sets, this means that a generation coefficient (g) value of approximately 0.1 corresponds to the borderline region where $n_s/g\tau_d \approx 1$. This borderline region correlates well with our results, and should account for the observed differences in PRIZ dynamics between low intensity exposures ($n_s/g\tau_d \approx 10$) and high intensity exposures ($n_s/g\tau_d \approx 0.001$). Therefore, the parameter $n_s/g\tau_d = 1$ defines a critical transition point in PRIZ dynamics, and must be accounted for in any interpretation of analytical results from our models. Accepting this, as well as the basic validity of our model, we can easily see why the cathode electric field never varies significantly from its initial value for low intensity exposures. Though photoionization, electron drift, and electron trapping enjoy an extremely short injection-free period in which to build a cathode electric field, the injection current quickly becomes dominant and then relaxes. The reasons the cathode field subsequently becomes less negative, indicating negative injection, are unclear. An adjustment of the boundary conditions for bin one or a modification of the equation modelling the injection current might eliminate this negative injection.

In spite of the difficulties mentioned above, we were still able to show that the net charge densities in all bins, except bin one, approach zero as the exposure continues. An intuitive analysis of the charge in bin one indicates that the only ways for this last remnant of net positive space charge to diminish is through donor recombination or

enhanced trapping. Both of these events are dependent on the density of free electrons in bin one. Analysis of the data for the normalized density of electrons in bin one, however, shows a minuscule value of 0.1, that is achieved almost immediately, and does not appear to vary at all over time. In comparison, the normalized density of electrons in bin 2 climbs to 8000 over the course of the exposure. Although we appear unable to affect this last remnant of charge in bin one, the following discussion indicates that we might be able to simply ignore it, and thereby claim success in one-dimensionally demonstrating self erasure. In a 1984 paper by Bryksin, he states, "The contribution from the positive space charge region to the transverse field for small z is therefore shielded more strongly, owing to mirror image forces on the negative electrode." (12:881) Petrov elaborates on this shielding effect near the cathode as follows:

> Contraction of the charge layer towards the electrode accompanied by slowing down of the charge density growth causes a decrease of the readout light modulation amplitude by virtue of the fact that the transverse components of the charge field near the electrode turn out to be weakened to a great extent by the field of the "mirror" charge produced by the electrode. (32:347)

If we accept these statements, then the charge density in bin one, and perhaps in bin two, should not modulate the read light to any great degree. Therefore, the response should eventually diminish with increasing exposure, indicating self erasure. Similar studies, using a progressively greater number of bins, could be used to confirm that the net positive space charge always retreats into the progressively smaller first bin. In the limit of infinitesimal bin size, a residual net

positive space charge exclusively in bin one would most definitely indicate self erasure in one dimension. Our analysis of self erasure neglects the catastrophic effects of dielectric breakdown as reported by Anderson (1:1). For high intensity self erasure data, we are well past the exposure value ($\mathcal{E} \approx 1.0$ mJ/cm^2) where this damage occurs (23:21).

We did not analyze the SI PRIZ at extremely high exposure values. Such an exercise could help isolate the effects of injection. Intuitively, we would expect the net positive space charge region in the SI PRIZ to also retreat to the first few bins, albeit at a slower rate. If these bins can indeed be disregarded, then the SI PRIZ, with no injection, would also exhibit self erasure.

VI. Conclusions and Recommendations

Our attempts to analytically reproduce qualitative aspects of Russian analytical data in the 1988 paper were highly successful. The quantitative differences in our analytical data and Russian analytical data, however, are inexplicable. Our models appear to accurately reproduce the effects of injection in the conducting PRIZ, however, some data was troubling. For example, the cathode electric fields at low intensity exposures consistently went less negative, indicating negative injection. This occurred in spite of the fact that the corresponding net space charge distribution indicated conditions favorable for the formation of an increased cathode electric field which should, in turn, result in injection. Other data indicated, however, that injection was indeed happening in spite of this apparent discrepancy. The extremely low values for free electron density in bin one, at extremely high exposure values, were also surprising. Overall, however, our models appear to require little modification. If there are errors, they probably reside in our modelling of bin one or its boundary conditions.

Reproduction of Russian experimental data was much less successful. Since experimental data on reciprocity and self erasure emerged as essentially multi-dimensional effects, we were not surprised that our one-dimensional models were somewhat inadequate. The Russians' failure to report specific experimental data and analytical parameters also hampered our efforts. Great benefit could be derived by repeating the Russian experiments, reported in the 1987 and 1988 papers, using PRIZ

crystals with known material parameters. Analysis of the results, using the models specified in this paper, might then prove more conclusive. Future researchers could also refine our models by including diffusion current, in addition to conduction and displacement current, in the term for total current. Refinements in injection modelling could resolve apparent inconsistencies in the behavior of the injection current for low intensity exposures. This might also result in more believable demonstrations of reciprocity and self erasure. A more sophisticated criterion for predicting transverse electric fields, and subsequent response, would also help in analyzing reciprocity and self erasure. Our crude criterion is rendered virtually useless, in many situations, because of its total disregard of the negative space charge region and the effects of the image charge.

The most obvious lesson learned from this report is that one-dimensional modelling is quickly approaching the point of diminishing returns. The very nature of the transverse electrooptic effect mandates the development of more sophisticated two-dimensional models. Accepting this, the computing power required by future AFIT PRIZ researchers can be expected to rise dramatically. Software upgrades will also be required since even our one-dimensional models often taxed the abilities of existing software.

Appendix: Landscape Plots

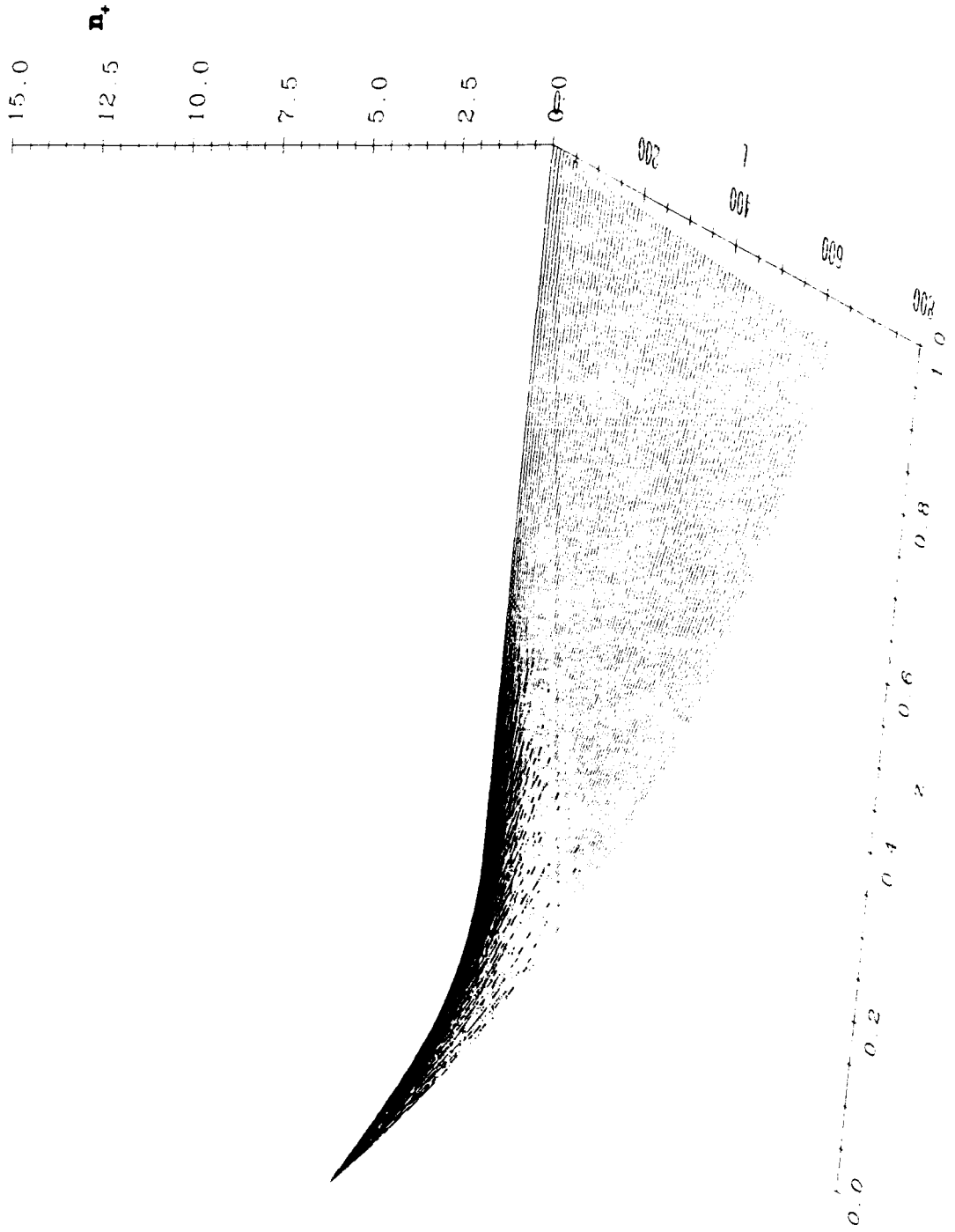

Figure 41. Density of Ionized Donors vs. Time and Distance for SI, Conducting, and DI PRIZ, $I' = 50\ \mu W/cm^2$, $n_s = 0$, 0.1, $\mathcal{E} = 0$ to 4 $\mu J/cm^2$

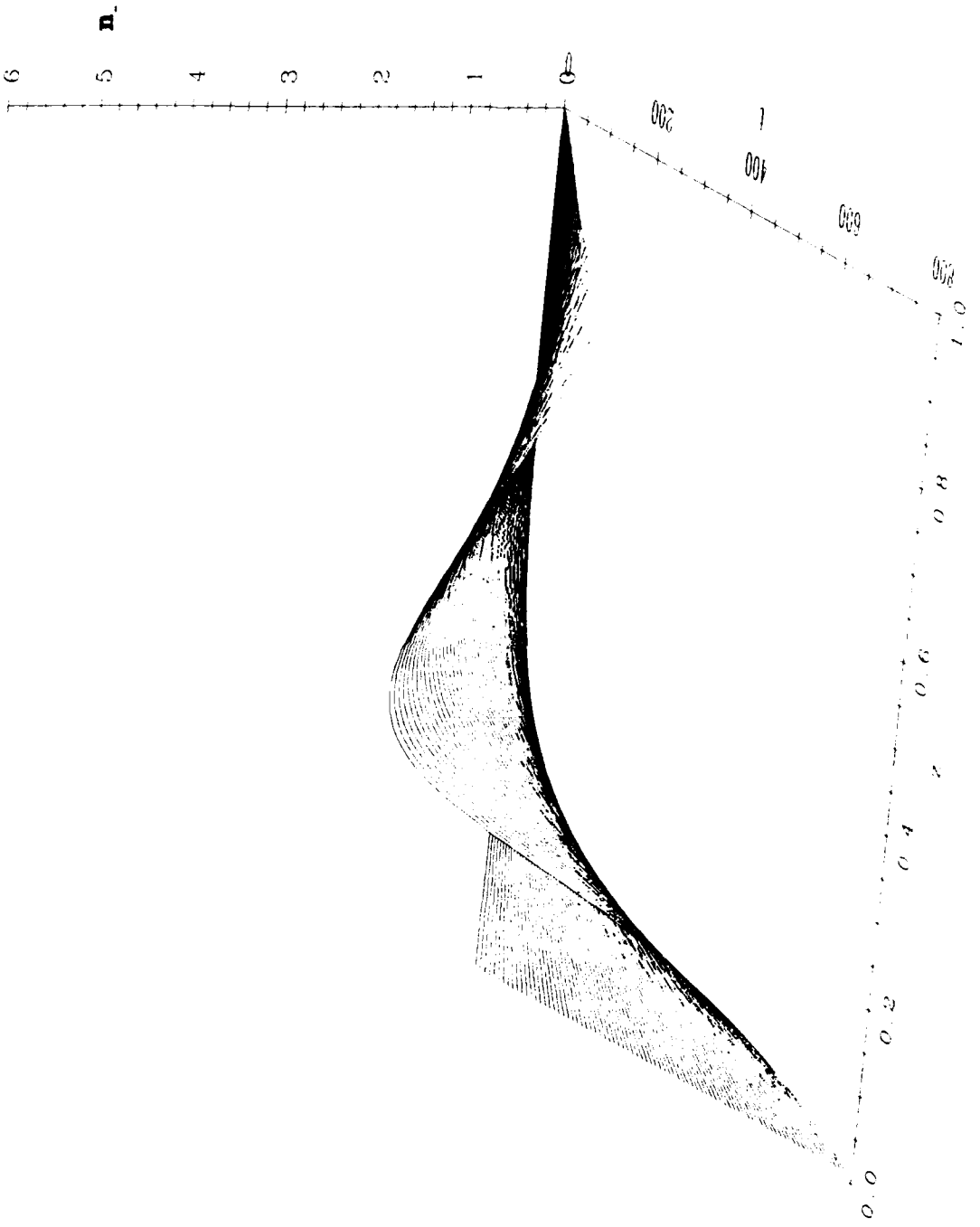

Figure 42. Density of Ionized Traps vs. Time and Distance, SI PRIZ, $I' = 50\ \mu W/cm^2$, $n_s = 0$, $\mathcal{E} = 0$ to 4 $\mu J/cm^2$

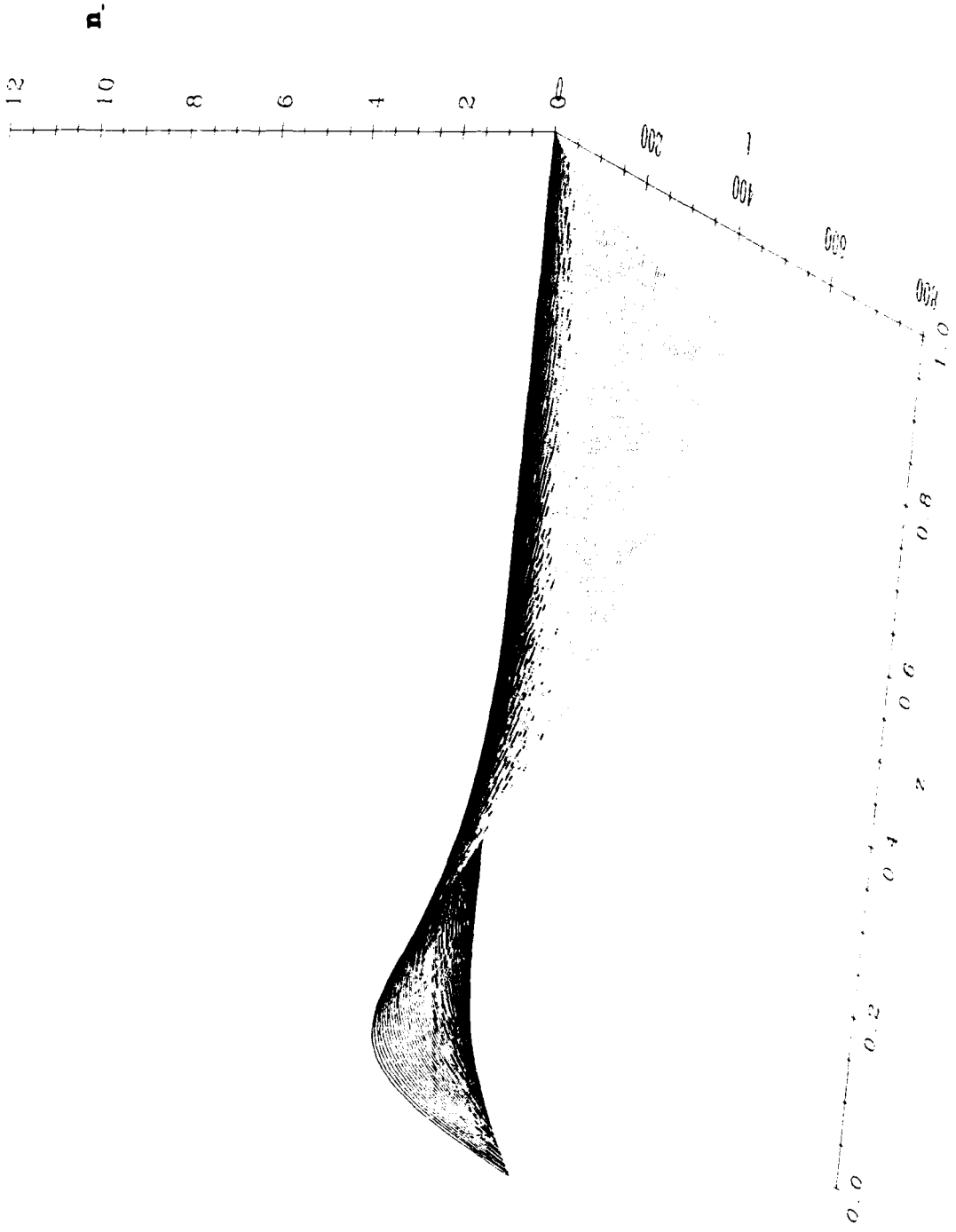

Figure 43. Density of Ionized Traps vs. Time and Distance, Conducting PRIZ, $I' = 50\ \mu W/cm^2$, $n_s = 0.1$, $\mathscr{E} = 0$ to $4\ \mu J/cm^2$

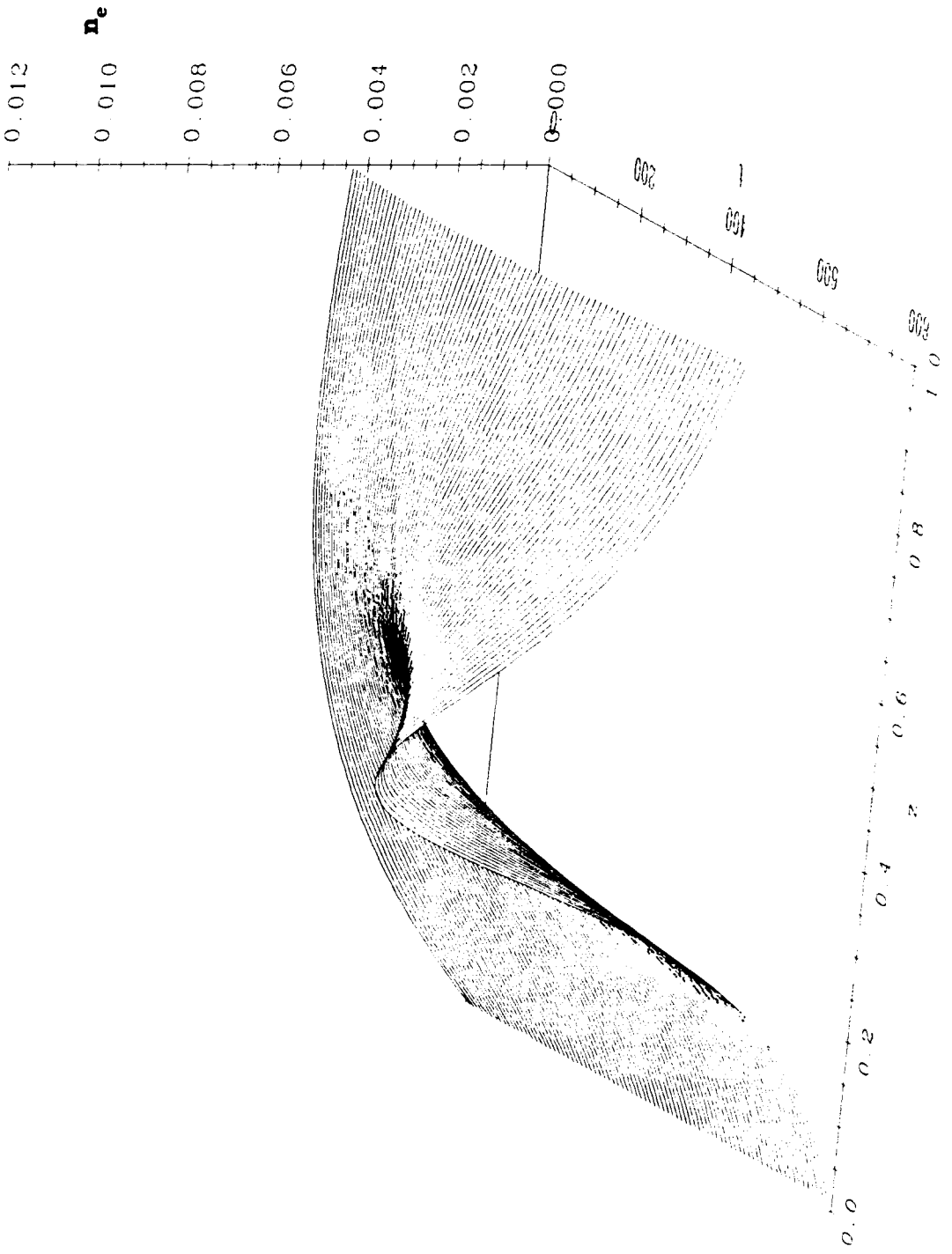

Figure 44. Density of Free Electrons vs. Time and Distance, SI PRIZ, $I' = 50\ \mu W/cm^2$, $n_s = 0$, $\mathcal{E} = 0$ to $4\ \mu J/cm^2$

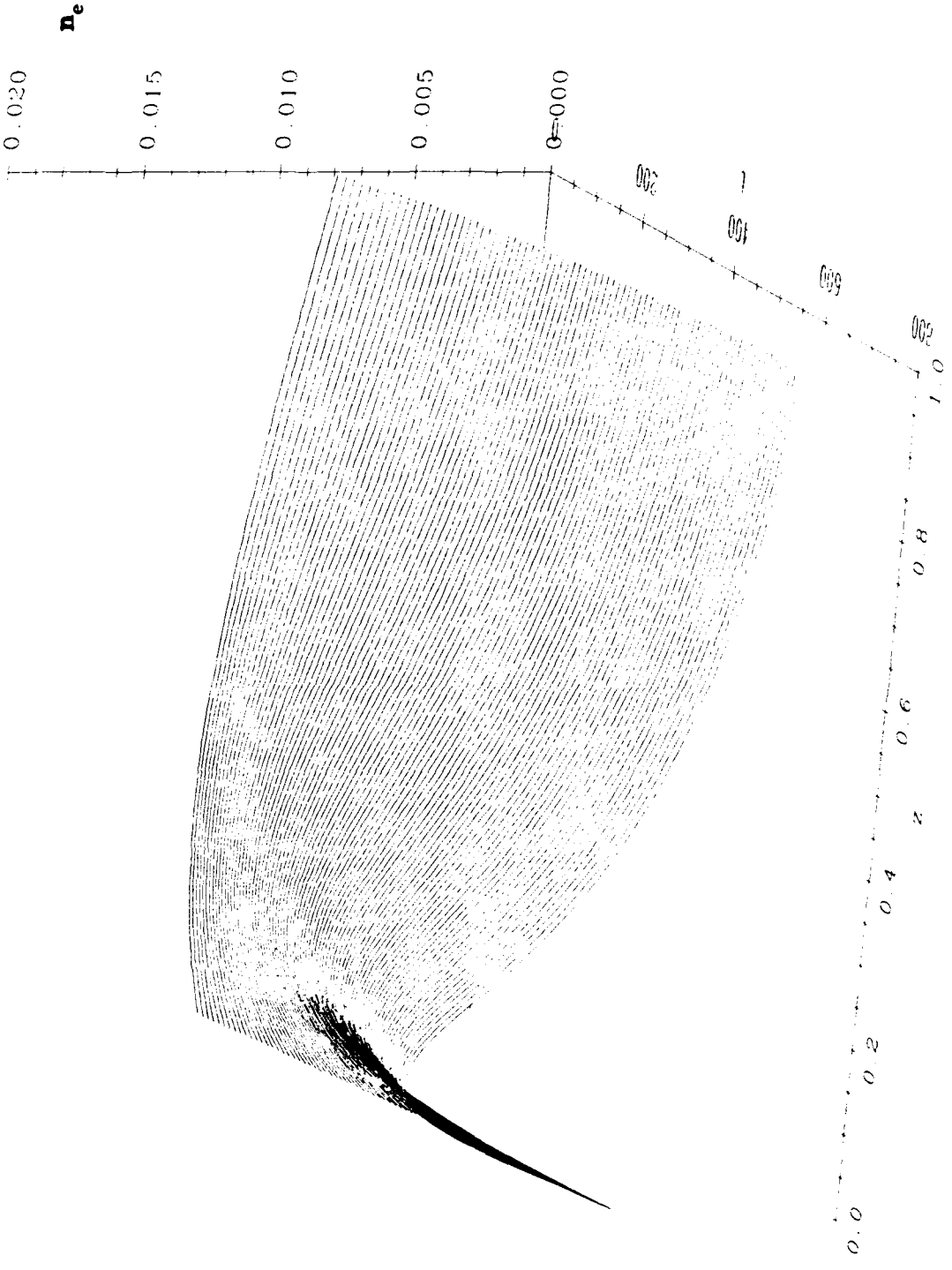

Figure 45. Density of Free Electrons vs. Time and Distance, Conducting PRIZ, $I' = 50\ \mu W/cm^2$, $n_s = 0.1$, $\mathcal{E} = 0$ to 4 $\mu J/cm^2$

Bibliography

1. Anderson, First Lt Danny L. Analysis of Write-Beam-Induced Damage on the Conducting PRIZ. MS thesis, AFIT/GEP/ENP/86D-1. School of Engineering, Air Force Institute of Technology (AU), Wright-Patterson AFB OH, December 1986 (AD-A170972).

2. Anderson, D. L. and T. E. Luke. "Write-Beam Induced Crystal Damage in the Conducting PRIZ," Optics Communications, 63: 78-80 (July 1987).

3. Astratov, V. N. et al. "Dynamics of the Distribution of the Field and Charge in $Bi_{12}GeO_{20}$ in the Case of Thermal Ionization of Traps," Soviet Physics Solid State, 25: 1585-1587 (September 1983).

4. Astratov, V. N. et al. "Stratification of the Space Charge in the Case of Screening of a Field in Crystals," Soviet Physics Solid State, 26: 1720-1725 (September 1984).

5. Bliznetsov, A. M. et al. "Injection Mechanism of Dynamic Image Selection in PRIZ Space-Time Light Modulators," Soviet Physics Technical Physics, 32: 750-754 (July 1987).

6. Bliznetsov, A. M. et al. "Investigation of Reciprocity in the PRIZ Space-Time Light Modulator," Soviet Physics Technical Physics, 33: 374-376 (March 1988).

7. Bryksin, V. V. et al. "Effect of Light Absorption on the Electric Field Distribution in $Bi_{12}SiO_{20}$," Soviet Physics Technical Physics, 9: 686-689 (June 1983).

8. Bryksin, V. V. et al. "Evolution of an Optically Induced Charge in the Case of Arbitrary Absorption of Light Including Capture by Traps," Soviet Physics Solid State, 28: 1528-1533 (September 1986).

9. Bryksin, V. V. et al. "Exact Solution of the Photoinduced Charge Formation Dynamics Problem in Photorefractive Crystals," Soviet Physics Solid State, 28: 79-83 (January 1986).

10. Bryksin, V. V. and L. I. Korovin. "Influence of Light Absorption on the Dynamics of Formation of Optically Induced Charges," Soviet Physics Solid State, 26: 2195-2199 (December 1984).

11. Bryksin, V. V. et al. "Initial Stage in the Redistribution of Photoinduced Charges and Electric Fields in $Bi_{12}SiO_{20}$," Soviet Physics Solid State, 24: 1686-1689 (October 1982).

12. Bryksin, V. V. et al. "Linear Operation of PRIZ Space-Time Light Modulators," Soviet Physics Technical Physics, 29: 878-882 (August 1984).

13. Bryksin, V. V. and L. I. Korovin. "Nonlinear Theory of the Dynamics of the Distribution of an Electric Field in Photorefractive Crystals," Soviet Physics Solid State, 25: 30-33 (January 1983).

14. Bryksin, V. V. and L. I. Korovin. "Photocurrent Oscillations and Nonlinear Electric Field Waves in Photorefractive Crystals," Soviet Physics Solid State, 26: 1487-1493 (August 1984).

15. Bryksin, V. V. et al. "Role of Electron Injection in the Formation of Optical Images in $Bi_{12}SiO_{20}$ Crystals," Soviet Technical Physics Letters, 9: 165-166 (April 1983).

16. Bryksin, V. V. and L. I. Korovin. "Role of Injection Currents in Dynamic Image Selection under Conditions Nonlinear in the Electric Field," Soviet Physics Solid State, 25: 1347-1351 (August 1983).

17. Bryksin, V. V. et al. "Role of Injection Currents in the Evolution of a Photoinduced Charge in Photorefractive Crystals," Soviet Physics Solid State, 29: 757-761 (May 1987).

18. Bryksin, V. V. and L. I. Korovin. "Role of Nonlinear Processes in Determining the Photoinduced Charge Near the Surface of Insulators," Soviet Physics Solid State, 26: 2051-2057 (November 1984).

19. Bryksin, V. V. et al. "Theory of Dynamic Image Selection in Photorefractive Media," Soviet Physics Solid State, 24: 193-196 (February 1982).

20. Casasent, David et al. "Applications of the Priz Light Modulator," Applied Optics, 21: 3846-3854 (November 1982).

21. Cushing, First Lt David A. A Numerical Analysis of the Dynamics of PRIZ Operation. MS thesis, AFIT/GEP/ENP/87D-5. School of Engineering, Air Force Institute of Technology (AU), Wright-Patterson AFB OH, July 1987 (AD-A188853).

22. Gardner, Capt Patrick J. Evaluation of the Spatial and Temporal Characteristics of the Conducting PRIZ. MS thesis, AFIT/GEO/ENP/88D-3. School of Engineering, Air Force Institute of Technology (AU), Wright-Patterson AFB OH, December 1988 (AD-A202530).

23. Gardner, P. J. and T. E. Luke. "The Spatial and Temporal Characteristics of the Conducting PRIZ Spatial Light Modulator," Optics Communications, 73: 19-22 (September 1989).

24. Günter, P. "Holography, Coherent Light Amplification and Optical Phase Conjugation with Photorefractive Materials," Physics Reports, 93: 199-299 (1982).

25. Horwitz, B. A. and F. J. Corbett. "The PROM - Theory and Applications for the Pockels Readout Optical Modulator," Optical Engineering, 17: 353-364 (July/August 1978).

26. Marrakchi, A. et al. "Physical Characterization of the Photorefractive Incoherent-to-Coherent Optical Converter," Optical Engineering, 24: 124-131 (January/February 1985).

27. Mints, G. and E. Tyugu. "The Programming System PRIZ," Journal of Symbolic Computation, 5: 359-375 (1988).

28. Nelson, Thomas E. Evaluation of One-Dimensional Mathematical Models of the Standard PRIZ. MS thesis, AFIT/ENP/GEO/90D-4. School of Engineering, Air Force Institute of Technology (AU), Wright-Patterson AFB OH, December 1990.

29. Nilius, Maj Mark E. Measurement and Analysis of the Memory Capabilities of a Conducting PRIZ. MS thesis, AFIT/GEO/ENP/85D-3. School of Engineering, Air Force Institute of Technology (AU), Wright-Patterson AFB OH, December 1985 (AD-A172418).

30. Peltier, M. and F. Micheron. "Volume Hologram Recording and Charge Transfer Process in $Bi_{12}SiO_{20}$ and $Bi_{12}GeO_{20}$," Journal of Applied Physics, 48: 3683-3690 (September 1977).

31. Petrov, Mikhail P. et al. "Light Pulse Response of Space-Time Light Modulators Using the Transverse Electrooptic Effect," Soviet Physics Technical Physics, 28: 823-826 (July 1983).

32. Petrov, Mikhail P. and A. V. Khomenko. "Photorefractive Crystals in PRIZ Spatial Light Modulators," Topics in Applied Physics, 62: 325-352 (1989).

33. Petrov, Mikhail P. et al. "The PRIZ Image Converter and its Use in Optical Data Processing Systems," Soviet Physics Technical Physics, 26: 816-821 (July 1981).

34. Petrov, Mikhail P. et al. "Spatial Modulation of Light in $Bi_{12}TiO_{20}$," Soviet Technical Physics Letters, 11: 106-107 (March 1985).

35. Petrov, Mikhail P. et al. "Transients in a Space-Time Light Modulator," Soviet Technical Physics Letters, 6: 165-166 (April 1980).

36. Shields, Capt Duncan M. Construction and Analysis of a PRIZ Spatial Light Modulator Exhibiting Dynamic Image Selection. MS thesis, AFIT/GEO/ENP/84D-4. School of Engineering, Air Force Institute of Technology (AU), Wright-Patterson AFB OH, December 1984 (AD-A152318).

37. Shlyagin, M. G. et al. "Mechanisms of Nonlinearity in a PRIZ Space-Time Light Modulator," Soviet Physics Technical Physics, 30: 68-72 (January 1985).

38. Sprague, Robert A. "Effect of Bulk Carriers on PROM Sensitivity," Journal of Applied Physics, 46: 1673-1678 (April 1975).

Vita

Captain Joseph W. Cook, III was born on 14 April 1958 in Chattanooga, Tennessee. He graduated from Hixson High School in Hixson, Tennessee in 1976 and attended the U.S. Air Force Academy, graduating with a Bachelor of Science in Engineering (specialty: Physics) in June 1980. Upon graduation, he received a regular commission in the USAF and attended pilot training. Prior to attending AFIT in May 1990, he served as a helicopter pilot and air operations staff officer in the 20th Special Operations Squadron and the 1st Special Operations Wing at Hurlburt Field, Florida.

Permanent Address: 1333 Cloverdale Dr.
Hixson, TN 37343

REPORT DOCUMENTATION PAGE

Form Approved
OMB No 0704-0188

1. AGENCY USE ONLY (Leave blank)	2. REPORT DATE	3. REPORT TYPE AND DATES COVERED
	December 1991	Master's Thesis

4. TITLE AND SUBTITLE
AN ANALYSIS OF ONE-DIMENSIONAL MODELS OF THE INSULATING AND CONDUCTING PRIZ

5. FUNDING NUMBERS

6. AUTHOR(S)
Joseph W. Cook, III, Captain, USAF

7. PERFORMING ORGANIZATION NAME(S) AND ADDRESS(ES)
Air Force Institute of Technology
Wright-Patterson AFB, OH 45433-6583

8. PERFORMING ORGANIZATION REPORT NUMBER
AFIT/GEP/~~ENG~~ENP/91D-2

9. SPONSORING MONITORING AGENCY NAME(S) AND ADDRESS(ES)

10. SPONSORING MONITORING AGENCY REPORT NUMBER

11. SUPPLEMENTARY NOTES

12a. DISTRIBUTION AVAILABILITY STATEMENT
Approved for public release; distribution unlimited

12b. DISTRIBUTION CODE

13. ABSTRACT (Maximum 200 words)

This study attempted to analytically reproduce experimental and analytical data, on the single-insulated and conducting PRIZ, presented in 1987 and 1988 by the Soviet scientists Bliznetsov et al. Previously successful codes were used to analyze the effects of injection at high and low intensity exposures (30 $\mu W/cm^2$ to 500 mW/cm^2). Although our codes qualitatively duplicated the nature of the space charge distribution in the single-insulated and conducting PRIZ, our quantitative results were significantly different from the Soviets'. Furthermore, the one-dimensional codes proved insufficient to effectively duplicate experimental data on reciprocity, self erasure, and regeneration. Specifically, we were unable to analytically reproduce Soviet experimental data establishing a reciprocity region for low exposures (< 20 $\mu J/cm^2$) in the conducting PRIZ. Since the basis for PRIZ operation, the linear electrooptic effect, is inherently a multi-dimensional phenomenon, we were not surprised to find some limitations to our one-dimensional models.

14. SUBJECT TERMS	15. NUMBER OF PAGES
PRIZ, Spatial Light Modulator, Spatial Time Light Modulator, STLM, PROM, Bismuth Silicate, BSO, Conducting PRIZ, Insulating PRIZ, Photorefractive Crystals	112
	16. PRICE CODE

17. SECURITY CLASSIFICATION OF REPORT	18. SECURITY CLASSIFICATION OF THIS PAGE	19. SECURITY CLASSIFICATION OF ABSTRACT	20. LIMITATION OF ABSTRACT
Unclassified	Unclassified	Unclassified	UL

GENERAL INSTRUCTIONS FOR COMPLETING SF 298

The Report Documentation Page (RDP) is used in announcing and cataloging reports. It is important that this information be consistent with the rest of the report, particularly the cover and title page. Instructions for filling in each block of the form follow. It is important to **stay within the lines to meet optical scanning requirements.**

Block 1. Agency Use Only (Leave Blank)

Block 2. Report Date. Full publication date including day, month, and year, if available (e.g. 1 Jan 88). Must cite at least the year.

Block 3. Type of Report and Dates Covered. State whether report is interim, final, etc. If applicable, enter inclusive report dates (e.g. 10 Jun 87 - 30 Jun 88).

Block 4. Title and Subtitle. A title is taken from the part of the report that provides the most meaningful and complete information. When a report is prepared in more than one volume, repeat the primary title, add volume number, and include subtitle for the specific volume. On classified documents enter the title classification in parentheses.

Block 5. Funding Numbers. To include contract and grant numbers; may include program element number(s), project number(s), task number(s), and work unit number(s). Use the following labels:

C	- Contract	**PR**	- Project
G	- Grant	**TA**	- Task
PE	- Program Element	**WU**	- Work Unit Accession No.

Block 6. Author(s). Name(s) of person(s) responsible for writing the report, performing the research, or credited with the content of the report. If editor or compiler, this should follow the name(s).

Block 7. Performing Organization Name(s) and Address(es). Self-explanatory.

Block 8. Performing Organization Report Number. Enter the unique alphanumeric report number(s) assigned by the organization performing the report.

Block 9. Sponsoring/Monitoring Agency Names(s) and Address(es). Self-explanatory.

Block 10. Sponsoring/Monitoring Agency. Report Number. (If known)

Block 11. Supplementary Notes. Enter information not included elsewhere such as: Prepared in cooperation with...; Trans. of ..., To be published in .... When a report is revised, include a statement whether the new report supersedes or supplements the older report.

Block 12a. Distribution/Availablity Statement. Denote public availability or limitation. Cite any availability to the public. Enter additional limitations or special markings in all capitals (e.g. NOFORN, REL, ITAR)

DOD	- See DoDD 5230.24, "Distribution Statements on Technical Documents."
DOE	- See authorities
NASA	- See Handbook NHB 2200.2.
NTIS	- Leave blank.

Block 12b. Distribution Code.

DOD	- DOD - Leave blank
DOE	- DOE - Enter DOE distribution categories from the Standard Distribution for Unclassified Scientific and Technical Reports
NASA	- NASA - Leave blank
NTIS	- NTIS - Leave blank.

Block 13. Abstract. Include a brief (Maximum 200 words) factual summary of the most significant information contained in the report.

Block 14. Subject Terms. Keywords or phrases identifying major subjects in the report.

Block 15. Number of Pages. Enter the total number of pages.

Block 16. Price Code. Enter appropriate price code (NTIS only).

Blocks 17. - 19. Security Classifications. Self-explanatory. Enter U.S. Security Classification in accordance with U.S. Security Regulations (i.e., UNCLASSIFIED). If form contains classified information, stamp classification on the top and bottom of the page.

Block 20. Limitation of Abstract. This block must be completed to assign a limitation to the abstract. Enter either UL (unlimited) or SAR (same as report). An entry in this block is necessary if the abstract is to be limited. If blank, the abstract is assumed to be unlimited.